Meas. Sci. Technol. **21** (2010) 102001 (29pp) doi:10.1088/0957-0233/21/10/102001

TOPICAL REVIEW

# Shearography technology and applications: a review

**D Francis[1,2], R P Tatam[2] and R M Groves[1]**

[1] Optical Non-Destructive Testing Laboratory, Faculty of Aerospace Engineering, Delft University of Technology, Kluyverweg 1, Postbus 5058, 2600 GB Delft, The Netherlands
[2] Department of Engineering Photonics, School of Engineering, Cranfield University, Cranfield, Bedford, MK43 0AL, UK

E-mail: r.p.tatam@cranfield.ac.uk and R.M.Groves@tudelft.nl

Received 10 February 2010, in final form 8 July 2010
Published 25 August 2010
Online at stacks.iop.org/MST/21/102001

**Abstract**
Shearography is a full-field speckle interferometric technique used to determine surface displacement derivatives. For an interferometric technique, shearography is particularly resilient to environmental disturbances and has hence become an invaluable measurement tool outside of the optics laboratory. Furthermore, the inclusion of additional measurement channels has turned shearography from a qualitative inspection tool into a system suitable for quantitative surface strain measurement. In this review article we present a comprehensive overview of the technique, describing the principle of operation, optical configurations, image processing algorithms and applications, with a focus on more recent technological advances.

**Keywords:** shearography, speckle interferometry, non-destructive testing, strain measurement

(Some figures in this article are in colour only in the electronic version)

## 1. Introduction

The measurement of strain and related parameters is important for many engineering disciplines. Knowledge of the behaviour of a component or structure under loading allows engineers to design new lightweight structures, to investigate forming and joining techniques, to introduce new materials and to validate computational solid mechanics models. Non-destructive testing is used in both the production environment for manufacturing quality control and during maintenance to guide the replacement of components for safety or performance. Strain measurement is conventionally performed using resistance strain gauges; however recent developments in optical instrumentation, e.g. shearography [1], digital image correlation [2] and fibre Bragg gratings [3], allow much more measurement flexibility.

Since its first demonstration [4], speckle shearing interferometry, or shearography [5], has offered the specific advantages of interferometric full-field displacement gradient sensitivity using an optical configuration inherently more resilient to environmental disturbances and vibrations than other interferometric techniques such as electronic speckle pattern interferometry (ESPI) [6]. As such it has become an important diagnostic tool, particularly in the field of non-destructive testing [7] where it has been used primarily for qualitative inspection, for example, to reveal delaminations in composite structures such as aircraft tyres and aircraft skins [8]. More recently, shearography has been developed to enable quantitative full surface strain measurement [9].

To make a measurement using shearography, the optically rough surface of the object under investigation is illuminated with laser light so that a speckle pattern is formed. The speckle pattern is imaged through a shearing device which coherently combines the speckle pattern with an identical but laterally displaced version of itself. This interferometric speckle pattern is then recorded by a CCD camera. Images are recorded before and after some loading event and correlation of these images results in a fringe pattern. The phase of the fringe pattern contains information on the displacement derivative of the surface and in order to make a quantitative measurement the

 

phase distribution across the image needs to be reconstructed. There are several techniques that have been used to do this but a common one, known as temporal phase stepping [10], involves recording a series of images with a known phase step between them. The images are combined to produce a wrapped phase map with a phase modulo $2\pi$. These wrapped phase fringe discontinuities can later be removed so that a continuous measurement is obtained. This process is known as phase unwrapping [11].

The aim of this review is to present a comprehensive overview of shearography, in particular the development that has led to its use as a quantitative inspection tool, starting with a discussion on theoretical aspects of various illumination configurations. The next section describes the different measurements that can be made using shearography, both static and dynamic, including strain measurement and shape/slope measurement as well as a description of recent technological advances and a range of different shearing devices that have been recently reported. The image processing requirements of shearography, including the different phase analysis techniques, phase unwrapping and filtering are presented in section 4, along with a discussion on the errors and uncertainties associated with the technique. The penultimate section presents some of the applications for which shearography has been employed, including a range of examples of its use for non-destructive testing. Examples of the use of quantitative multi-component shearography, including a system utilizing pulsed illumination and fibre-optic imaging bundles [12], are also presented as well as some micro-scale applications and some examples of commercially available systems.

## 2. Theoretical overview

In this section the theory of operation of shearography is discussed. To begin with, a simple single measurement channel shearography system predominantly sensitive to out-of-plane displacement derivative is described. Then more complex configurations that can be used to measure in-plane displacement derivative and all three surface strain components are discussed. In all the systems described in this section a Michelson interferometer is used as the shearing device, since this is commonly used. Other shearing devices can be used and these are discussed in section 3.5.

### *2.1. Out-of-plane displacement gradient measurement*

The optical arrangement of a shearography system suitable for measurement of out-of-plane displacement gradient is shown in figure 1. The output of a laser is expanded to illuminate the region of interest of the surface of the object under investigation. The scattered light forms a laser speckle pattern which is imaged through a Michelson shearing interferometer, onto a CCD camera. The shearing device serves to divide the image so that two identical, but displaced, images are recorded by the CCD camera. The two images combine coherently producing an interferometric speckle pattern at the sensor of the camera. A typical laser speckle pattern is

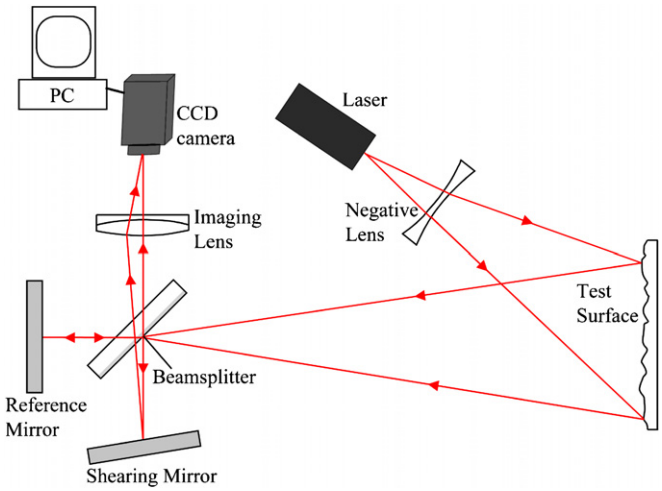


**Figure 1.** A shearography system based on a Michelson shearing interferometer. The instrument is sensitive to a single component of displacement gradient predominantly in the out-of-plane direction.

shown in figure 2(*a*). The light contributing to each speckle in the pattern is scattered from points on the objects surface separated by the shear distance. Any subsequent deformation of the surface will result in a variation in the phase difference between the light scattered from those points resulting in a change in intensity of each speckle. A comparison of images recorded before and after some loading event, commonly by digital subtraction and rectification, results in a fringe pattern where the fringes represent a locus of points with the same magnitude of displacement gradient. A typical correlation fringe pattern obtained from a point out-of-plane displacement of a flat plate is shown in figure 2(*b*). The approximate magnitude of displacement gradient along the white horizontal line through figure 2(*b*) is indicated in the graph in figure 2(*c*).

Consider a point on the object's surface, located at the point $P(x, y, z)$, as shown in figure 3. Light from the source $S(x_S, y_S, z_S)$ is scattered from $P$ and imaged onto a point on the detector at $D(x_D, y_D, z_D)$ via one of the two paths through the shearing device. After the object has been deformed, the point $P$ is displaced to the position $P'(x+u, y+v, z+w)$, where $(u, v, w)$ is the displacement vector at the point $P$. The displacement vector and its relationship with the $(x, y, z)$ coordinate system is also shown in figure 3. The origin of the coordinate system is located on the object surface at the centre of the field of view of the camera and the out-of-plane direction $z$ is in the direction of the camera from the object.

The change in optical path length for $P$ due to the deformation is given by

$$\Delta L_P = (SP' + P'D) - (SP + PD) \tag{1}$$

where [13]

$$\begin{aligned} SP &= ((x - x_S)^2 + (y - y_S)^2 + (z - z_S)^2)^{1/2} \\ PD &= ((x - x_D)^2 + (y - y_D)^2 + (z - z_D)^2)^{1/2} \\ SP' &= ((x + u - x_S)^2 + (y + v - y_S)^2 + (z + w - z_S)^2)^{1/2} \\ P'D &= ((x + u - x_D)^2 + (y + v - y_D)^2 + (z + w - z_D)^2)^{1/2} \end{aligned} \tag{2}$$

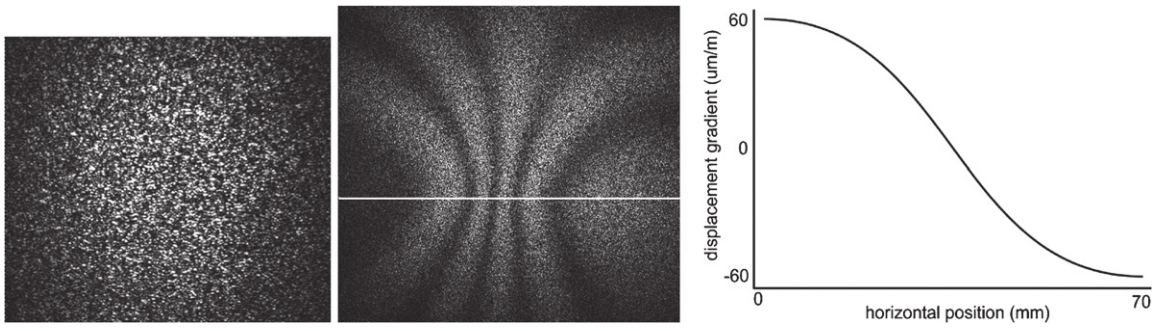


**Figure 2.** A typical laser speckle pattern (*a*), a correlation fringe pattern obtained using an out-of-plane sensitive shearography system (*b*) and the approximate displacement gradient versus horizontal position along the white line (*c*).

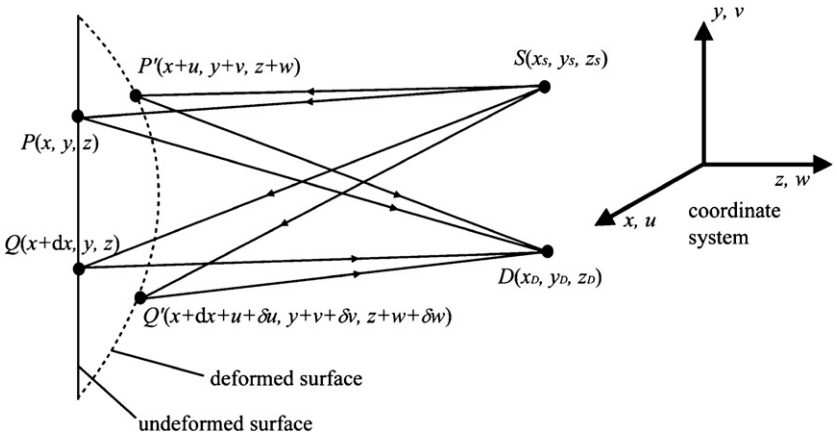


**Figure 3.** Diagram showing the optical paths between the source $S$ and detector $D$ for two points on the object's surface, $P$ and $Q$ separated by the shear distance d$x$, before and after object deformation. The coordinate system shows that $u$, $v$ and $w$ are the displacement components in the $x$, $y$ and $z$ directions, respectively [13].

using a binomial expansion and taking only the first-order terms we obtain [13]

$$\Delta L_P = \left(\frac{x - x_D}{R_D} + \frac{x - x_S}{R_S}\right) u + \left(\frac{y - y_D}{R_D} + \frac{y - y_S}{R_S}\right) v + \left(\frac{z - z_D}{R_D} + \frac{z - z_S}{R_S}\right) w \tag{3}$$

where

$$R_D = \left(x_D^2 + y_D^2 + z_D^2\right)^{1/2} \quad \text{and} \quad R_S = \left(x_S^2 + y_S^2 + z_S^2\right)^{1/2} \tag{4}$$

Substituting the relationships

$$A = \frac{x - x_D}{R_D} + \frac{x - x_S}{R_S}, \quad B = \frac{y - y_D}{R_D} + \frac{y - y_S}{R_S} \quad \text{and} \quad C = \frac{z - z_D}{R_D} + \frac{z - z_S}{R_S} \tag{5}$$

into (3) we obtain

$$\Delta L_P = Au + Bv + Cw. \tag{6}$$

Light arriving at the point at $D(x_D, y_D, z_D)$ is scattered from the object surface at point $P$ and the point $Q$, also shown in figure 3, which travels along the other path through the shearing device and is separated from $P$ by the shear distance d$x$. After deformation the point $Q(x + \mathrm{d}x, y, z)$ is displaced to $Q'(x + \mathrm{d}x + u + \delta u, y + v + \delta v, z + w + \delta w)$ where $u + \delta u$, $v + \delta v$ and $w + \delta w$ are the $x$, $y$ and $z$ components of the displacement vector at the point $Q$. The change in optical path length for $Q$ due to the deformation is found in the same way as before:

$$\Delta L_Q = A(u + \delta u) + B(v + \delta v) + C(w + \delta w). \tag{7}$$

The relative optical path between the two points is found by subtracting equations (6) and (7):

$$\Delta L_Q - \Delta L_P = A\delta u + B\delta v + C\delta w. \tag{8}$$

If the shear d$x$ is small, the displacement difference approximates to the displacement gradient and the optical phase difference can be written as

$$\Delta\phi = \frac{2\pi}{\lambda}\left(A\frac{\partial u}{\partial x} + B\frac{\partial v}{\partial x} + C\frac{\partial w}{\partial x}\right)\mathrm{d}x. \tag{9}$$

The factors $A$, $B$ and $C$ are sensitivity factors dependent on the observation and illumination directions and are equivalent to the components of the sensitivity vector $\mathbf{k} = (k_x, k_y, k_z)$ which is defined as the bisector of the observation and illumination vectors. Equation (9) can therefore be rewritten as

$$\Delta\phi = \frac{2\pi}{\lambda}\left(k_x\frac{\partial u}{\partial x} + k_y\frac{\partial v}{\partial x} + k_z\frac{\partial w}{\partial x}\right)\mathrm{d}x. \tag{10}$$

If the $k_x$ and $k_y$ components of the sensitivity vector are brought close to zero then the contributions from

the in-plane displacement derivatives are minimized and the system becomes predominantly sensitive to the out-of-plane displacement gradient component. This is achieved in practice by making the observation and illumination directions close to collinear. In this case, the out-of-plane displacement derivative is given by [14]

$$\frac{\partial w}{\partial x} = \frac{\lambda \Delta\phi}{4\pi\, \mathrm{d}x} \tag{11}$$

and when the shear is applied in the $y$-direction the out-of-plane displacement component is given by [14]

$$\frac{\partial w}{\partial y} = \frac{\lambda \Delta\phi}{4\pi\, \mathrm{d}y}. \tag{12}$$

### 2.2. In-plane displacement gradient measurement

In shearography, in-plane displacement derivatives can be measured using an optical system that possesses two symmetrical illumination directions. The object is simultaneously illuminated by both beams, and a fringe pattern is produced due to the coherent combination of the two beams. The fringe pattern that is generated is sensitive to the $\partial u/\partial x$ displacement gradient component, assuming shear in the $x$-direction, if the beams lie in the $x$–$z$ plane or the $\partial v/\partial x$ displacement gradient component if the beams lie in the $y$–$z$ plane. Using this technique results in an additional interference pattern being produced due to the shearing interferometer that is located between the object and the camera. The subsequent moiré effect between the two sets of fringes results in in-plane displacement gradient-sensitive fringes that are of poor contrast [15].

An alternative method [16, 17] of isolating the in-plane displacement derivatives also uses symmetrical illumination but instead involves illuminating with each illumination *sequentially*. Images are recorded for each illumination direction before and after object deformation and the phase distribution is then calculated for each. Subtracting the results obtained for each illumination direction results in the out-of-plane component being minimized, isolating the in-plane component. The in-plane strain measured using shear in the $x$-direction and illumination directions in the $x$–$z$ plane is given by [15]

$$\frac{\partial u}{\partial x} = \frac{\lambda(\Delta\phi_{+\theta} - \Delta\phi_{-\theta})}{4\pi \sin\theta\, \mathrm{d}x} \tag{13}$$

where $\theta$ is the angle between the object surface normal and the illumination direction.

### 2.3. Multi-component measurement

If the illumination direction of a shearography instrument does not lie in the $x$–$z$ plane or the $y$–$z$ plane, then the resulting measurements contain contributions from all three displacement derivative components. It is therefore possible to isolate all three displacement derivative components using an instrument with three illumination directions with different directional sensitivities [18–20]. It is also possible, as we shall see later, to use three observation directions. A typical three-component shearography system based on three illumination directions is shown in figure 4.

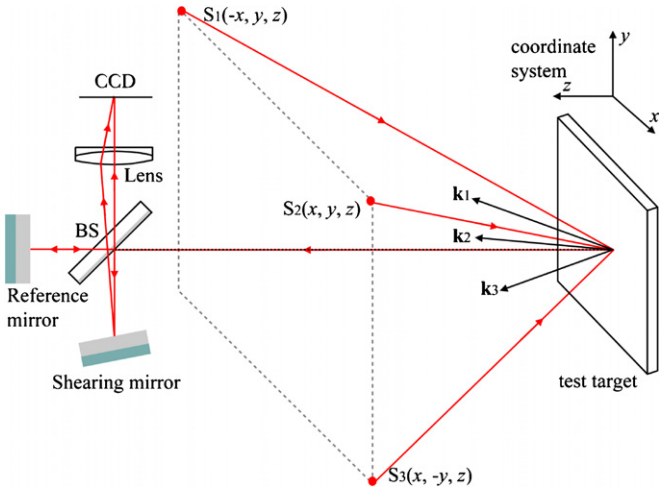


**Figure 4.** A multi-component shearography system with three sources located at positions $S_1$, $S_2$ and $S_3$. BS refers to the beamsplitter in the shearing interferometer. The sensitivity vectors of the measurement channels formed by the three sources are given by $\mathbf{k}_1$, $\mathbf{k}_2$ and $\mathbf{k}_3$.

The three optical sources are positioned at three of the corners of a square at locations $S_1(-x, y, z)$, $S_2(x, y, z)$ and $S_3(x, -y, z)$. The optical phase difference measured using each of the measurement channels is given by

$$\begin{aligned}
\Delta\phi_{S1} &= \frac{2\pi}{\lambda}\left(k_{x1}\frac{\partial u}{\partial x} + k_{y1}\frac{\partial v}{\partial x} + k_{z1}\frac{\partial w}{\partial x}\right)\mathrm{d}x \\
\Delta\phi_{S2} &= \frac{2\pi}{\lambda}\left(k_{x2}\frac{\partial u}{\partial x} + k_{y2}\frac{\partial v}{\partial x} + k_{z2}\frac{\partial w}{\partial x}\right)\mathrm{d}x \\
\Delta\phi_{S3} &= \frac{2\pi}{\lambda}\left(k_{x3}\frac{\partial u}{\partial x} + k_{y3}\frac{\partial v}{\partial x} + k_{z3}\frac{\partial w}{\partial x}\right)\mathrm{d}x
\end{aligned} \tag{14}$$

where the numerical subscripts refer to the measurement channels formed by sources 1–3, respectively. These equations can be written as a matrix and the displacement derivatives are then given by

$$\begin{bmatrix} \frac{\partial u}{\partial x} \\ \frac{\partial v}{\partial x} \\ \frac{\partial w}{\partial x} \end{bmatrix} = \frac{\lambda}{2\pi} \begin{bmatrix} k_{x1} & k_{y1} & k_{z1} \\ k_{x2} & k_{y2} & k_{z2} \\ k_{x3} & k_{y3} & k_{z3} \end{bmatrix}^{-1} \begin{bmatrix} \Delta\phi_{S1} \\ \Delta\phi_{S2} \\ \Delta\phi_{S3} \end{bmatrix} \mathrm{d}x^{-1}. \tag{15}$$

The strain tensor $S$ is given by [9]

$$\begin{aligned}
S &= \begin{bmatrix} \varepsilon_x & \gamma_{xy} & \gamma_{xz} \\ \gamma_{yx} & \varepsilon_y & \gamma_{yz} \\ \gamma_{zx} & \gamma_{zy} & \varepsilon_z \end{bmatrix} \\
&= \begin{bmatrix} \boxed{\frac{\partial u}{\partial x}} & \boxed{\frac{1}{2}\left(\frac{\partial u}{\partial y} + \frac{\partial v}{\partial x}\right)} & \frac{1}{2}\left(\frac{\partial u}{\partial z} + \boxed{\frac{\partial w}{\partial x}}\right) \\ \boxed{\frac{1}{2}\left(\frac{\partial v}{\partial x} + \frac{\partial u}{\partial y}\right)} & \boxed{\frac{\partial v}{\partial y}} & \frac{1}{2}\left(\frac{\partial v}{\partial z} + \boxed{\frac{\partial w}{\partial y}}\right) \\ \frac{1}{2}\left(\boxed{\frac{\partial w}{\partial x}} + \frac{\partial u}{\partial z}\right) & \frac{1}{2}\left(\boxed{\frac{\partial w}{\partial y}} + \frac{\partial v}{\partial z}\right) & \frac{\partial w}{\partial z} \end{bmatrix}
\end{aligned} \tag{16}$$

where $\varepsilon_x$, $\varepsilon_y$, $\varepsilon_z$ are the normal strain components and $\gamma_{xy}$, $\gamma_{xz}$, $\gamma_{yx}$, $\gamma_{yz}$, $\gamma_{zx}$, $\gamma_{zy}$ are the shear strain components. The boxed displacement derivative quantities represent those

which can be measured using shearography. The other quantities represent the bulk strain components and cannot be measured using shearography since this would require a measurement into the volume of the object. Shearography is therefore limited to measurement only of the surface strain of object under investigation, since the bulk strain components do not contribute to this.

## 3. Measurements and technological advances

In this section the use of multi-component shearography for quantitative surface strain measurement that was introduced in section 2.3 is discussed further. We also describe how shearography can be used for profiling of non-planar objects, a requirement for quantitative measurements of surface strain, and discuss the use of shearography for dynamic measurements such as the analysis of vibrating and rotating objects and dynamic loading events such as impact and shock. This section also covers some of the recent technological advancements such as the shearing devices, polarization-based systems and the use of incoherent illumination. The impact of recent improvement in components such as cameras, laser systems and computers is also discussed.

### *3.1. Quantitative surface strain measurement*

Strain had traditionally been measured with the resistance strain gauge, which although simple and effective, is subject to a number of limitations. In particular, the strain gauge only measures the surface strain at a single point, with the spatial resolution dependent on the size (gauge length) of the gauge, and also it needs to be physically adhered to the surface of the object under investigation which, in many situations, is not trivial. Optical techniques overcome these problems by providing non-contact measurements over the field of view of the imaging system. Of the optical techniques, shearography is particularly appealing due to its measurement sensitivity to the derivative of surface displacement, a parameter closely related to strain.

Full surface strain characterization can be achieved through the measurement of six displacement derivative components, two out-of-plane and four in-plane. This can be achieved using shearography instrumentation with at least three measurement channels and two orthogonal shear directions. Multi-component surface strain analysis was first reported by Steinchen *et al* [17, 21]. This was done using a configuration similar to that shown in figure 1 to measure the out-of-plane strains and the dual-illumination configuration that was discussed in section 2.2 to measure the in-plane strains. The triple-illumination-direction configuration described in section 2.3 was suggested by Aebischer and Waldner [22]. This configuration can be used to simultaneously measure and isolate two in-plane strain components and one out-of-plane strain component. Later practical multiple illumination systems were developed by James and Tatam [18], Waldner and Brem [19] and Kästle, Hack and Sennhauser [20]. The systems described in [18] and [19] multiplexed signals from the different measurement channels temporally. In [20] frequency multiplexing was achieved using three sources with different wavelengths and wavelength selective components to discriminate between signals. Using this method image acquisition from each channel is simultaneous; however, accurate pixel registration is required between each of the three cameras and the optical system is complex. In order to measure non-planar surfaces a correction needs to be made to compensate for the variation of the shear magnitude and the sensitivity vector due to the shape of the object [23]. The derivative of an object's shape can be measured with shearography and techniques to achieve this will be described in section 3.2.

The $\partial x$ and $\partial y$ strain components are frequently obtained by repeating measurements with orthogonal shear directions. A method of shear direction multiplexing was presented by Groves *et al* [24]. The light from a diode laser was coupled into a highly birefringent (hi-bi) optical fibre with each of the eigenaxes of the fibre equally populated. This was achieved by converting the linearly polarized output of the laser to circularly polarized light with a quarter-wave plate. Laser diode wavelength modulation was used to switch between orthogonal linear polarization states of the light exiting the hi-bi fibre. A polarization-sensitive beamsplitter located in one arm of a Michelson interferometer was used to guide the light to the vertically or horizontally aligned mirror depending on the polarization state. Frequency modulation of the laser diode was also used for the purpose of phase analysis.

So far only multi-component shearography systems with multiple illumination directions have been discussed. Equivalently, systems can be developed with a single illumination direction and multiple observation directions. This can be done using multiple cameras and shearing interferometers positioned to give different directional sensitivities. An alternative configuration involves the use of coherent fibre-optic imaging bundles to transport images from the various observation positions to a single interferometer and camera [12]. Previously endoscopic shearography has been demonstrated [25], though only using a single component for qualitative measurements. Additional considerations with multiple-observation-direction configurations that are not required in multiple-illumination-direction systems include the need for adequate image registration between measurements from the various channels and errors due to perspective distortions arising because of the oblique viewing angles. A multiple-observation-direction shearography system is shown in figure 27. These difficulties can be overcome using an appropriate image-dewarping algorithm [26]. One of the advantages of the multiple-observation-direction configurations is that the instrument can be used in conjunction with a high power laser system that may otherwise be too bulky or expensive to use in the multiple-illumination-direction configuration.

### *3.2. Object slope measurement*

Quantitative surface strain measurement of non-planar objects requires a correction due to the shape of the object. This can be achieved with a measure of the shape of the object.

Shearography is suitable for the measurement of object slope, the derivative of shape. The use of shearography for surface profiling has been reviewed by Shang *et al* [27]. The principal techniques are the dual-wavelength method [28], object rotation [29] and source displacement [30].

In the dual-wavelength technique the object is illuminated at an initial wavelength $\lambda_1$ and an image is recorded. The object is then illuminated again at a second wavelength $\lambda_2$ and another image is recorded. The images are subtracted and a correlation fringe pattern is obtained with fringes contouring the slope of the object. The separation of the contour fringes is proportional to the magnitude of the equivalent wavelength $\lambda_{eq}$ given by

$$\lambda_{eq} = \frac{\lambda_1 \lambda_2}{|\lambda_1 - \lambda_2|}. \tag{17}$$

The wavelength shift can be achieved in a practical system through frequency modulation of a laser diode. As an example, in [28], frequency shifts of 88 GHz ($\Delta\lambda = 0.2$ nm) and 132 GHz ($\Delta\lambda = 0.3$ nm) resulted in contour spacing of 3.4 mm and 2.3 mm, respectively.

In the rotation method the object is rotated by a small amount between exposures and a correlation fringe pattern is obtained through subtraction of the two images. Assuming normal observation, the object slope is related to the phase of the fringe pattern by

$$\frac{\partial z}{\partial x} = -\frac{\Delta\phi\lambda}{2\pi\,(\Delta\alpha \sin\beta)\,\mathrm{d}x} \tag{18}$$

where $\Delta\alpha$ is the angle of rotation and $\beta$ is the illumination angle. Good contrast fringe patterns were obtained in [29] using a rotation angle of 0.017°.

Another technique involves displacement of the optical source. This method can be useful since the object rotation technique may not be suitable for large objects and the dual-wavelength technique requires good laser frequency stability. The source displacement technique involves displacing the optical source in a direction perpendicular to the illumination axis between exposures and producing a correlation fringe pattern through digital subtraction. The translation needs to be done carefully since any translation along the illumination axis will introduce carrier fringes which will distort the slope-sensitive fringes [30]. Quantitative shape measurements from a cylindrical pipe were made in [30] by calculating the phase using temporal phase stepping. The unwrapped phase measurements were referenced against unwrapped phase measurements from a flat plate and scaled using a calculated slope sensitivity constant.

Anand *et al* [31] used a Fresnel wavefront propagation model to simulate shape measurement with source displacement in shearography. The results of the simulation showed improved accuracy compared to measurements that had previously been measured using shearography. However, the Fresnel propagation model was computationally intensive which meant that only very small simulated objects were investigated. Figure 5(*a*) shows a wrapped phase map generated with the model from a simulated cone with a base diameter of 4 mm and a height of 50 $\mu$m. The angle of illumination was set at 36°. The flat plate phase map against which the cone measurement was referenced is shown in figure 5(*b*). The two-phase maps shown in figures 5(*a*) and (*b*) were subtracted and the result was unwrapped and is shown in figure 5(*c*). Figures 5(*d*) and (*e*) show the simulated and measured slope and shape, respectively.

### *3.3. Dynamic measurements*

Shearography can be used to determine the derivative of vibrational amplitudes of surfaces [32]. If the vibration is harmonic and significantly faster than the frame rate of the camera, then time-averaged measurements can be made using continuous wave illumination. When making time-averaged measurements image pairs are continuously recorded and correlated by subtraction, a process known as sequential subtraction. This is in contrast to the static subtraction used with conventional shearography where images are subtracted from a single reference image. A $\pi$ phase shift between the pairs of images is required since the difference in average intensity would be zero over many vibrational cycles [33]. A fringe pattern is then obtained with an intensity distribution given by [32]

$$I_{ave}(x, y) \propto J_0^2\left(\frac{4\pi}{\lambda}\frac{\partial A(x, y)}{\partial x}\,\mathrm{d}x\right) \tag{19}$$

where $A$ is the amplitude of vibration and $J_0$ is the zero-order Bessel function. The result of following this function is that there is one fringe in the pattern, known as the nodal, or Bessel fringe, which is bright and the intensity of the fringes drops off significantly away from this fringe. In shearography, the nodal fringe is located at the positions of maximum vibration amplitude. Heterodyning of the system by laser frequency modulation can be used to shift the position of the Bessel fringe within the pattern [34], as shown in figure 6. Examples of time-averaged fringes obtained from a vibrating thermal protection tile from the NASA space-rescuecraft X38 programme are shown in figure 7. Using stroboscopic illumination converts the Bessel fringes to cosinusoidal fringes which have uniform intensity across the fringe pattern [35]. This has been utilized to effectively measure ultrasonic waves propagating through aluminium bars [36]. Further, synchronization of the repetition rate of the laser with the vibrational frequency can allow phase recovery through the temporal phase-stepping technique.

The measurement of high-speed transient deformations presents further difficulties since the time-averaged method is no longer suitable and therefore continuous wave illumination cannot be used. The dual-pulse technique is often used for transient measurements. In this technique, the object is illuminated by a laser pulse with a duration that is much shorter than the deformation rate of the object, thus effectively freezing its motion [35]. The object is illuminated by a second laser pulse a short time afterwards and the relative deformation is measured by the subtraction of images recorded from the two pulses. One of the major issues with the dual-pulse method is in the phase analysis. Due to the nature of the deformation, the conventional temporal phase-stepping technique cannot be used since there is not sufficient time to record the phase-stepped images. The phase therefore needs to be recovered from two images only. Typically carrier fringe

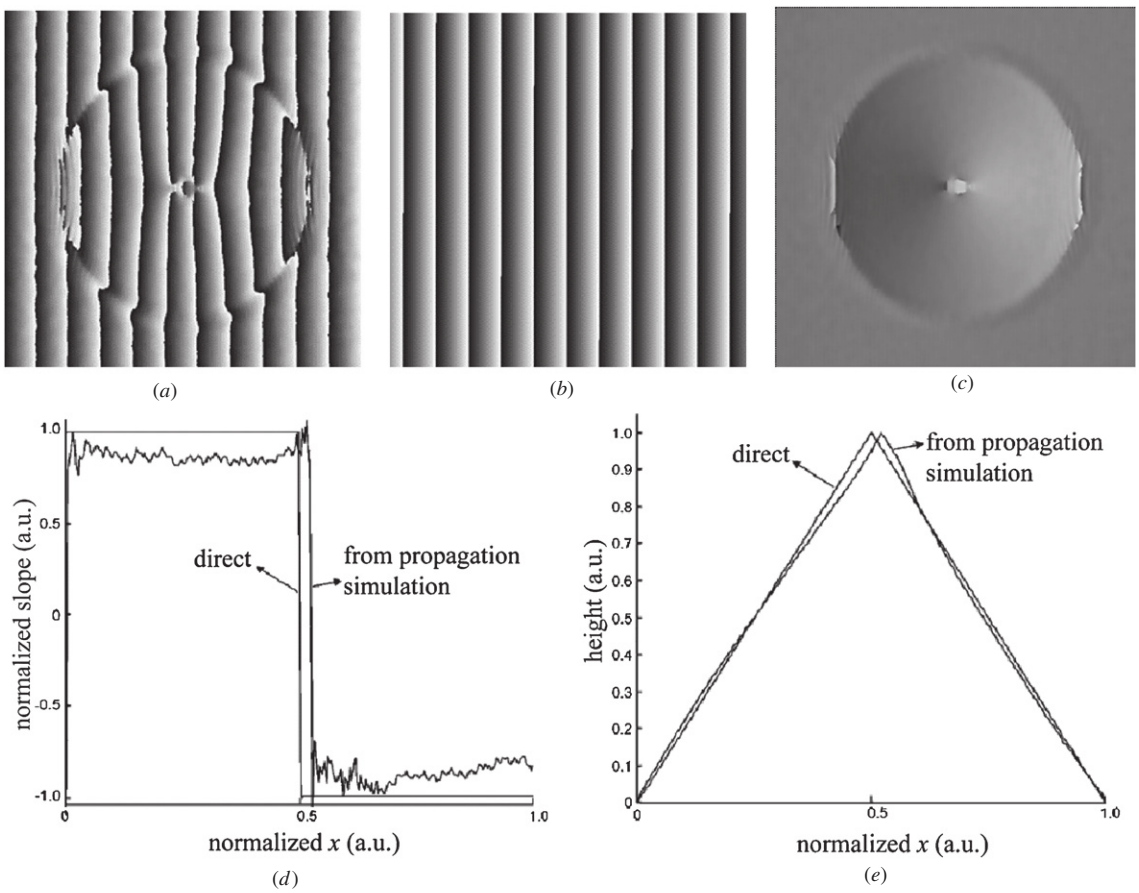


**Figure 5.** Wrapped phase maps produced by the Fresnel wavefront propagation model for a simulated cone (*a*) and a flat plate (*b*). (*c*) The unwrapped difference of (*a*) and (*b*). The comparison of measured and simulated slope (*d*) and shape (*e*) [31].

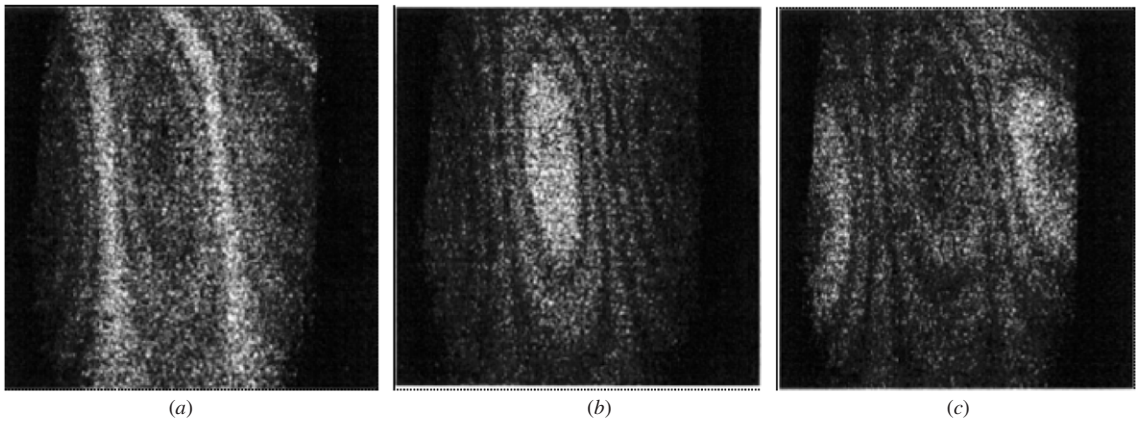


**Figure 6.** Time-averaged Bessel fringes from a gas turbine blade vibrating at 5.6 kHz (*a*). Heterodyned fringes with a relative phase shift of $\pi/2$ are shown in (*b*) and (*c*) [34].

techniques using Fourier transform phase demodulation are used. This problem is discussed further in section 4.2. Some of the applications of pulsed shearography are presented in section 5.2.

### *3.4. Other measurements*

*3.4.1. Displacement measurement.* Shearography can be used to measure surface displacement. One method involves introducing a large image shear [38] so that one of the sheared images is not of the object under investigation at all but of a static reference surface. The method is analogous to ESPI, another interferometric speckle technique that is sensitive to surface displacement [39], but retains the stability benefits of shearography. This technique has been used in the measurement of residual stress [40].

*3.4.2. Curvature measurement.* Measurement of flexural strains and curvatures requires the measurement of

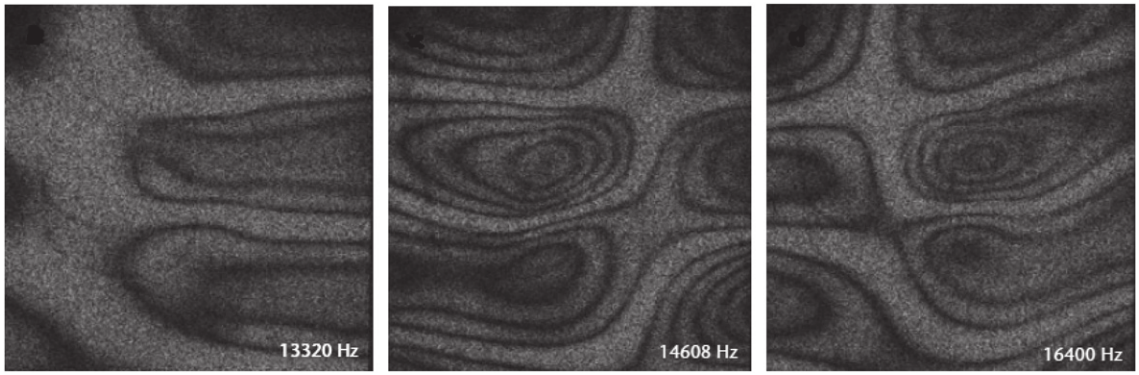


(*a*) (*b*) (*c*)

**Figure 7.** Time-averaged fringes obtained using an ISI-SYS™ shearography system from a vibrating thermal protection tile from the NASA space-rescuecraft X38 program [37].

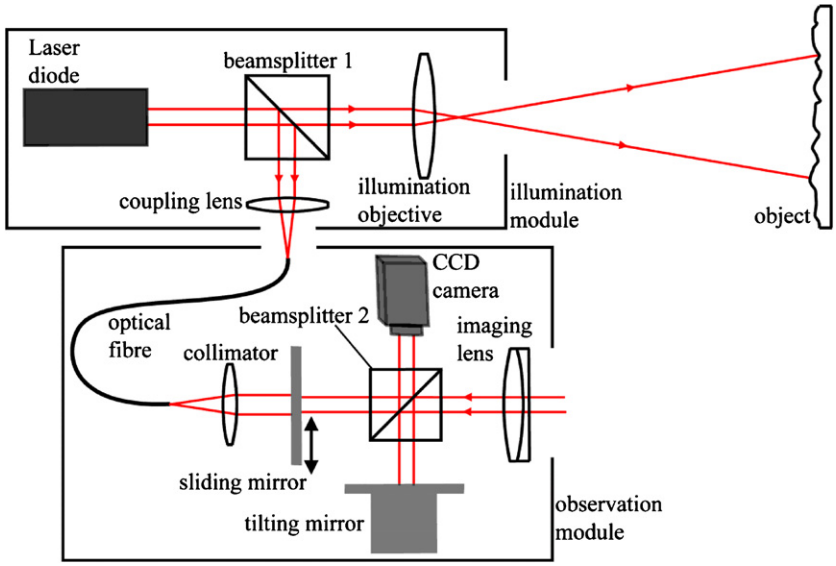


**Figure 8.** Optical arrangement of a combined shearography and ESPI instrument [47].

second-order displacement derivatives. To do this a number of techniques have been reported including multi-exposure shearography [41], a shearography configuration with three apertures [42] and an instrument with two Michelson shearing interferometers in series [43]. In the multi-exposure approach, images are recorded with the object unloaded and after loading. The third image is recorded after a slight lateral translation of the object and then the fourth image is recorded after the loading has been removed. The images are combined and the curvature fringes are observed as a moiré effect between two sets of displacement derivative fringes. In the three-aperture approach the central aperture is filled with a glass plate and the other two are filled with glass wedges to produce three sheared wavefronts. The use of dual Michelson interferometers also produces three sheared wavefronts. In the multiple aperture and dual interferometer approaches the object translation is not necessary and only two exposures are necessary. Wang *et al* [44] describe the influence of displacement and displacement derivative on the curvature measurements. Bhaduri *et al* [45] describe a technique to introduce carrier fringes by blocking successive apertures in a three-aperture shearography system. The phase of the curvature fringes can then be determined with a Fourier transform. Alternatively, a conventional Michelson shearing interferometer has been used with a continuous wavelet transform to determine the phase and the second-order derivatives [46].

*3.4.3. Combination with other optical techniques.* A number of authors have reported combining shearography with other techniques; in particular ESPI is a popular choice. This enables simultaneous measurement of surface displacement and displacement derivative from a single loading event using a single optical instrument.

In [38] large image shearing was used to produce ESPI measurements using the reflection from a static surface as a reference beam. The same instrument was also used with smaller image shear for conventional shearography measurements. Fomitchov and Krishnaswamy [47] describe the design of an optical system for both ESPI and shearography. A sliding mirror in the imaging head can be used to switch between ESPI and shearography functionality. A schematic of their optical system is shown in figure 8.

Shearography has also been combined with digital speckle photography [48]. Speckle photography is an image correlation-based technique typically used for measurement of in-plane displacement. Because of the nature of the technique it is sensitive to in-plane displacements a few orders of magnitude greater than that of ESPI or holographic interferometry. Combining shearography with speckle photography therefore allows three-component strain measurement (through numerical differentiation of the in-plane displacement measurements) using a single illumination and observation direction. This configuration would therefore be advantageous over multi-component configurations in situations where optical access is restricted. Recently Rosso *et al* [49] presented preliminary results of a combined holography and shearography arrangement that allows simultaneous coherent imaging and strain measurement. The instrument shows the potential for depth-resolved strain measurement inside optically diffusing biological tissue.

### *3.5. Shearing devices*

The Michelson interferometer is a popular choice of shearing device since it is simple to set up, offers easy adjustment of the image shear, and phase analysis through the temporal phase-stepping technique can be easily implemented by mounting one of the mirrors on a piezo-electric transducer (PZT). One of the drawbacks with the Michelson interferometer is its limited light efficiency since at least 50% of the light entering the interferometer is lost due to the dual pass through the beamsplitter. Alternative shearing devices include the image shearing camera [13] which has a glass wedge in one half of the camera's aperture, or the use of glass plates or a Fresnel bi-prism [15]. These devices have improved light efficiency compared to the Michelson though phase stepping is not so straightforward to implement. Another system that offers improved light efficiency relative to the Michelson interferometer utilizes the hi-bi optical fibre and a Wollaston prism [32, 50]. The orthogonal polarization modes of the fibre are equally populated and light exiting the fibre illuminates the surface under investigation. The reflected light is imaged onto the camera by a pair of lenses between which the prism is located. The prism is aligned such that a pair of sheared images corresponding to the two polarization modes of the fibre is produced. The magnitude of the image shear can be adjusted by translating the prism along the optical axis. A length of the optical fibre is coiled around a piezoelectric cylinder which is used as a phase modulator. Applying a voltage to the cylinder strains the fibre and induces a relative phase shift between the two orthogonally polarized modes.

Recently, a number of systems incorporating alternative shearing devices have been reported. Mihaylova *et al* [51] present a shearography system employing a pair of plane glass plates with different coefficients of reflection positioned in series. The second of the two plates is mounted to a PZT to facilitate phase shifting. The separation between the two plates determines the magnitude of the image shear. This instrument is shown schematically in figure 9(*a*). Another shearing mechanism involves using a photopolymer holographic grating in transmission [52], shown in figure 9(*b*). A sheet of ground glass positioned between the grating and the CCD camera serves to eliminate unwanted diffraction orders and remove the requirement to resolve the pitch of the grating.

Zhao and Chung [53] describe the use of a liquid crystal spatial light modulator (SLM) to introduce image shearing, as shown in figure 9(*c*). The SLM is programmed to simulate a binary phase grating which acts as the shearing device. Additionally temporal phase shifting is realized by shifting the grating pattern between frames. Since no additional moving parts are required to incorporate phase shifting, the instrument is free from uncertainties arising from miscalibration, hysteresis or thermal drift.

Rosso *et al* [54] describe an instrument that uses a prism with a glass plate as the shearing device, shown in figure 9(*d*). The back face of the prism has a coating which splits the incident wavefront into orthogonally polarized waves that are reflected and transmitted, respectively. The transmitted component is directed back towards the CCD camera using a thin glass plate fixed to the prism with the result that the two orthogonally polarized wavefronts are laterally sheared with respect to each other. The magnitude of the shear can be altered by using different thickness glass plates or by adjusting the separation between the prism and the imaging lens. A liquid crystal variable retarder located between the imaging lens and the CCD camera was used to facilitate phase shifting. Being an almost common-path interferometer, the system is particularly insensitive to environmental disturbances. Also, due to the in-line arrangement, the instrument is sensitive almost entirely to the out-of-plane component of displacement derivative, with minimal contributions from the in-plane components. Another configuration that has been reported involves using a glass wedge in reflection and obtaining sheared images from the reflections from the front and back surfaces [55]. This configuration has been demonstrated for non-destructive evaluation.

Although the systems presented here offer alternatives to the Michelson shearing interferometer, it does however retain a number of advantages; in particular it is straightforward to construct and temporal phase stepping is easily incorporated by mounting one of the mirrors onto a piezo-electric element.

### *3.6. Low coherence shearography*

Shearography has relatively low coherence requirements relative to other interferometric techniques due to the comparatively short differences in the optical paths through the interferometer. This has allowed the use of low coherence sources in shearography provided that the spatial coherence is sufficient to generate a speckle pattern. Falldorf *et al* [56] demonstrated that a mercury arc lamp can be used as the optical source in shearography. The instrument is currently limited by the small range of deformation and objects that can be investigated; however shearography fringe patterns were observed as shown in figure 10. Wang and Tieu [57] also describe the use of a low coherence source in shearography. A mercury lamp was used to measure the out-of-plane displacement derivative of a centrally loaded flat plate.

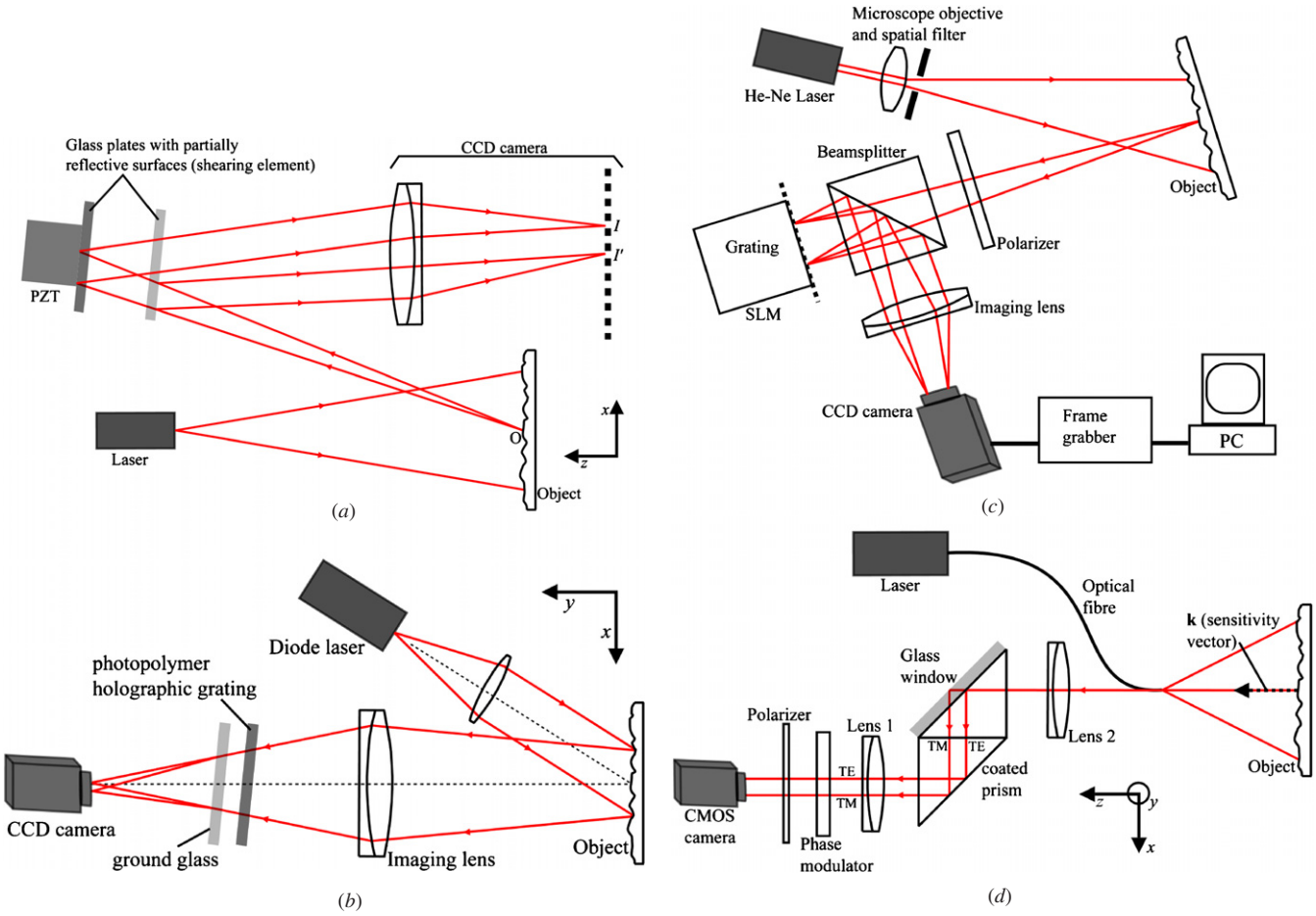


**Figure 9.** Some of the recently reported shearing interferometers with alternative shearing devices. A pair of glass plates (*a*) [51], a holographic grating and ground glass (*b*) [52], a spatial light modulator (SLM) (*c*) [53] and a prism with a coating and a glass plate (*d*) [54].

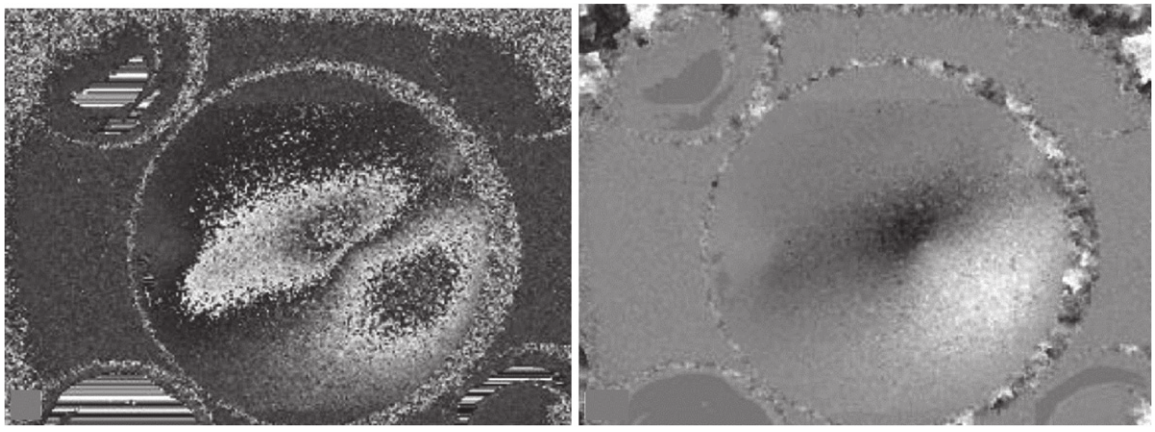

(*a*) (*b*)

**Figure 10.** Wrapped (*a*) and unwrapped (*b*) phase maps obtained using a mercury arc lamp as the illuminating source [56]. The field of view of the images is approximately 30 mm × 20 mm.

### *3.7. Improved technologies*

The rapid improvement in the associated electronics and optics means that development of simple digital shearography systems is now easier than ever before and more complex systems covering a wider range of measurement applications can be constructed. More powerful and coherent laser systems mean that larger objects can be investigated and transient deformations can be monitored. More compact laser systems simplify the construction of multiple measurement shearography systems suitable for quantitative three-component strain measurement. Improved camera resolution and bit depth allows for higher resolution measurements and high speed cameras based on CMOS

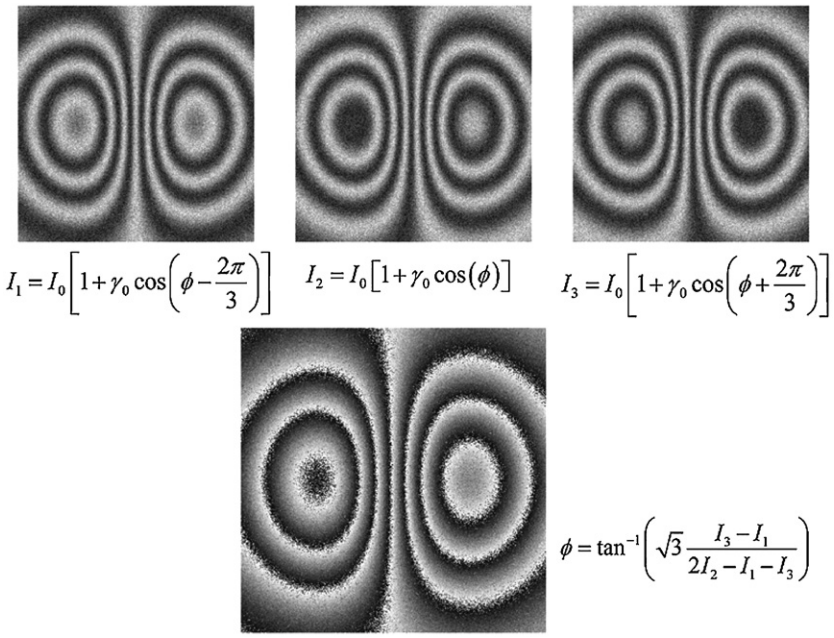


**Figure 11.** A series of simulated correlation fringe patterns with a relative phase step of $2\pi/3$ between them (top row) are combined using the three-step algorithm to produce a phase map wrapped in the range $-\pi$ to $+\pi$ (lower image.)

detectors even allow for analysis of dynamic surfaces, as has been demonstrated previously with ESPI [58]. Increased camera flexibility allows on-the-fly adjustment of camera parameters, e.g. integration time, allowing techniques such as extended dynamic range imaging in shearography [59]. The rapid development of PC hardware and software now allows for quasi-real-time image capture and display of both wrapped and unwrapped phase maps [60].

## 4. Phase analysis techniques and uncertainty evaluation

Reconstruction of the optical phase variation due to object deformation is an essential step in the process of making quantitative measurements with shearography since the phase is proportional to the measurand. Correlation of two speckle patterns results in an intensity-based fringe pattern that does not provide the phase information leading to the need for image processing procedures to recover this information. In this section, a range of phase analysis techniques are discussed including the commonly used temporal phase-stepping technique as well as other methods that can be used when the phase needs to be determined from a single frame only, such as in the measurement of dynamic events. The fringe patterns obtained with shearography tend to be of lower contrast than those generated with out-of-plane ESPI due to the combination of two speckle fields, as opposed to the combination of a speckle pattern and smooth reference. This was demonstrated by Slettemoen in the development of ESPI systems with speckle reference beams [61]. The image processing steps are described as well as post-processing procedures such as image filtering and phase unwrapping. Finally, some of the errors and uncertainties associated with shearographic measurements are discussed.

### *4.1. Phase stepping*

Temporal phase stepping involves recording a series of images with a known phase step between them. These images are then combined on a pixel-wise basis using a phase-stepping algorithm producing a wrapped phase map where the pixel values are bound between $-\pi$ and $+\pi$. In a Michelson shearing interferometer, phase shifting is often incorporated by mounting one of the mirrors on a PZT. Applying a voltage to the PZT shifts the mirror altering the relative path lengths in the interferometer, thus shifting the phase. Other phase modulation devices [10] include tilting a glass plate, rotating a wave plate or translating a diffraction grating. Phase shifting can also be achieved by frequency modulation using a path-length imbalanced interferometer [62]. The intensity distribution in a recorded fringe pattern at each pixel $(x, y)$ can be described by

$$I(x, y) = I_0(x, y)\{1 + \gamma_0(x, y)\cos[\phi(x, y)]\} \tag{20}$$

where $I_0$ is the background intensity, $\gamma_0$ is the fringe modulation function and $\phi$ is the phase. Since there are three unknowns in (20), a minimum of three fringe patterns is required to determine the phase. A series of three simulated fringe patterns with a relative phase of $2\pi/3$ between them is shown in figure 11. These fringe patterns can be combined using the three-step algorithm,

$$\phi = \tan^{-1}\left(\sqrt{3}\frac{I_3 - I_1}{2I_2 - I_1 - I_3}\right), \tag{21}$$

to yield a wrapped phase map. Other commonly used phase-stepping algorithms are the four-step algorithm [63], the five-step algorithm [64] and the Carré algorithm [65], which is also four steps, each of which requires images with a relative phase

step of $\pi/2$:

$$\phi_{4-\text{step}} = \tan^{-1}\left(\frac{I_4 - I_2}{I_1 - I_3}\right)$$

$$\phi_{5-\text{step}} = \tan^{-1}\left[\frac{2(I_2 - I_4)}{2I_3 - I_5 - I_1}\right]$$

$$\phi_{\text{Carre}} = \tan^{-1}\left\{\frac{\sqrt{[(I_1 - I_4) + (I_2 - I_3)][3(I_2 - I_3) - (I_1 - I_4)]}}{(I_2 + I_3) - (I_1 + I_4)}\right\}. \quad (22)$$

The three-step algorithm is the fastest of those presented since only three frames are required; however, the others offer additional benefits. For instance, the five-step algorithm compensates for errors introduced by miscalibration of the phase shifter and the Carré algorithm does not require known phase steps provided that they are close to $\pi/2$ and are equal.

Phase stepping can be applied to the reference frame only, with intermediate determination of phase shifted fringe patterns, or to both the reference and signal frames, where the wrapped phase map is determined solely from speckle patterns. The former is known as the 'phase of differences' approach and the latter is known as the 'difference of phases' approach [66]. The phase of differences method is faster, since only one signal frame needs to be acquired, but the difference of phase technique results in wrapped phase maps with less noise and higher contrast fringes.

### 4.2. Spatial phase stepping

The temporal phase-stepping technique discussed above is the preferred method of phase analysis for most shearography applications because it is straightforward to implement and produces wrapped phase maps with good spatial resolution. However, in some cases the measurand may vary during the time taken to record the phase-stepped images, resulting in an inaccurate measurement. This is the case when dynamic or transient measurements are to be made. One solution is to record a series of phase-stepped images simultaneously, a technique known as spatial phase stepping. This can be done using multiple cameras [67] which can be expensive and require complex optical arrangements. An alternative is to simultaneously record phase-stepped images with different regions of a single CCD camera. This has been achieved with ESPI using a diffractive optical element [68] and in a commercial system (4D Technology™) using a pixelated phase mask [69]. Phase maps obtained using this method will have reduced spatial resolution compared to temporal phase stepping since each image occupies only a fraction of the available area on the camera's sensor, although this may not be too much of a problem if a large format sensor is used. Another system that employs spatial phase shifting involves a polarization-based shearing interferometer which divides an incoming image into two and images them side-by-side on a camera with a $\pi$ relative phase shift [70]. Analysis showed that maintaining sub-pixel image registration was essential to maintain accurate measurements [71]. A more recent paper [70] discusses an improvement of the system when dealing with unfavourable polarization states.

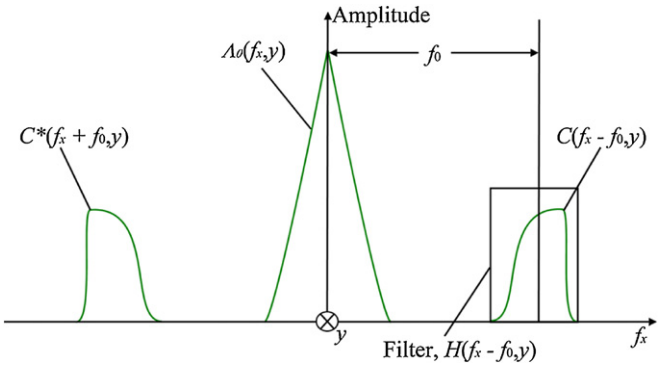


**Figure 12.** One-dimensional representation of the Fourier transform of a carrier fringe pattern.

### 4.3. Spatial carrier technique

The spatial carrier technique [72] is another process that can be used to determine the phase distribution from a single recording. In the spatial carrier technique a carrier frequency is introduced into the recorded intensity distribution which serves to separate the phase information from the background information in frequency space. The image can then be interrogated with a Fourier transform to isolate and calculate the phase distribution. The intensity of a carrier fringe pattern can be defined as

$$I(x, y) = I_0(x, y) + \gamma_0(x, y)\cos[\phi(x, y) + 2\pi f_0 x] \quad (23)$$

where $f_0$ is the carrier frequency. The interferogram can then be weighted with a window such as a Hamming or Hanning window to remove the influence of the discontinuities at edges of the data range. The intensity of the fringe pattern can be rewritten as

$$I(x, y) = I_0(x, y) + c(x, y)\exp(2\pi \mathrm{i} f_0 x) + c^*(x, y)\exp(-2\pi \mathrm{i} f_0 x) \quad (24)$$

where

$$c(x, y) = \frac{\gamma_0(x, y)}{2}\exp[\mathrm{i}\phi(x, y)] \quad (25)$$

and the $^*$ represents the complex conjugate. The one-dimensional Fourier transform of (24) with respect to the $x$-axis is

$$\Lambda(f_x, y) = \Lambda_0(f_x, y) + C(f_x - f_0, y) + C^*(f_x + f_0, y) \quad (26)$$

where $\Lambda$, $\Lambda_0$ and $C$ are the frequency space representations of $I$, $I_0$ and $c$, and $f_x$ is the spatial frequency in the $x$-direction. A one-dimensional representation of (26) is shown in figure 12.

The point at the centre contains the zero order term, which is equal to the sum of all values in the original fringe pattern and can consequently be very large relative to other values in the transformed spectrum. Surrounding the zero order term is the background distribution $\Lambda_0(f_x, y)$. The phase information is encoded in the two side terms separated equidistant from the zero order term by the carrier frequency $f_0$. A filter function $H(f_x - f_0, y)$ is used to isolate one of the side spectra and translate it back to the origin, thereby removing the carrier

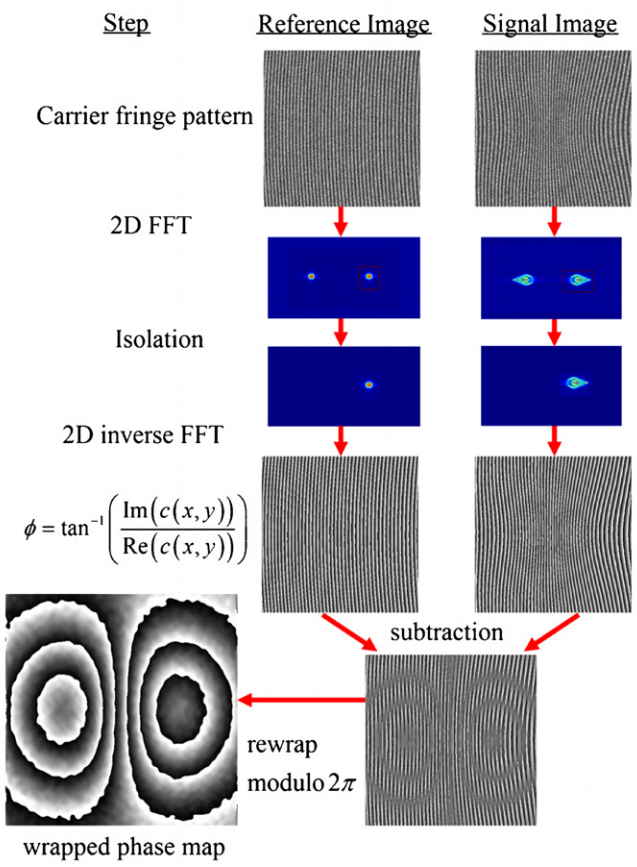


**Figure 13.** Sequence of processing steps used to calculate the phase difference from images using the spatial carrier technique, after [72].

frequency. An inverse Fourier transform is applied to the isolated and translated spectrum from which the phase can be determined using

$$\phi(x, y) = \tan^{-1}\left\{\frac{\mathrm{Im}[c(x, y)]}{\mathrm{Re}[c(x, y)]}\right\}. \tag{27}$$

The technique can be extended to two-dimensional fringe patterns but it requires that the carrier frequency is constant across the image, i.e. the carrier fringes need to be perfectly straight. This can be difficult to achieve in a practical shearography system. Any curvature in the fringes will be unrecognizable from the distortion in the fringes due to the phase modulation and therefore result in an erroneous measurement.

An alternative approach [73] is illustrated in figure 13 using simulated fringe patterns. A carrier fringe pattern is recorded with the object in its undeformed state. Note here that the carrier fringes are slightly curved. When a deformation is applied to the object a phase variation is induced resulting in a modulation of the carrier fringes. The Fourier transform of the reference and signal carrier fringe patterns is calculated, the magnitude of a region of the centre of which is shown. The average intensity of the two carrier fringe patterns is zero, therefore there is no zero order or background term in figure 13. One of the side features in each is isolated but in this case no translation is applied. The inverse Fourier transform is calculated and the phase is determined using equation (27). The phases calculated from the reference and signal images are subtracted and the result is rewrapped modulo $2\pi$ to yield the wrapped phase map. This technique works well and is convenient for determining the phase from a pair of fringe patterns. It is also more resilient to high frequency noise than the phase-stepping technique (compare with the wrapped phase map in figure 11). However, since it is a global technique as opposed to the pixel-wise operation of temporal phase stepping, pixels will have some influence on each other manifesting as the distortions within the fringe boundaries in the wrapped phase map in figure 13. This problem worsens as noise increases and can blur out high frequency fringes. In shearography the fringe density for a particular strain variation can be reduced by reducing the image shear.

One method of generating a carrier frequency in shearography is to translate the optical source along the optical axis between two exposures [74]. The difference in the two exposures results in a carrier fringe pattern where the frequency of the fringes is dependent on the magnitude of the translation. This can be realized practically by translating a diverging lens within the illumination path but this can be difficult to achieve in dual-pulsed shearography where the separation of pulses can be as short as 1 $\mu$s. A solution to this problem was presented by Fernández *et al* [75]. In their configuration, shown in figure 14, dual pulses are generated from twin Nd:YAG laser cavities. Pulses from the two cavities traverse different paths before being made collinear at beamsplitter 2 and illuminating the object. The amount of divergence of the two laser pulses is different due to the different positions of the negative lenses L1 and L2. Carrier fringe patterns can then be produced through the subtraction of speckle patterns recorded from the two pulses. An alternative design involves the use of a Pockels cell and polarization optics to direct the beams along separate paths via the two lenses L1 and L2 [76][3].

One of the drawbacks of this approach is the difficulty in obtaining a high enough carrier frequency to fully separate the phase-dependent terms from the background term in frequency space whilst maintaining good contrast carrier fringes. Another issue is that at least three images are required if the phase referencing procedure discussed above (figure 13) is to be used, which is problematic for dual-pulsed measurements. The method whereby the spectral feature is translated to the origin would only require two images; however perfectly straight carrier fringes would need to be produced.

Another technique used for carrier frequency generation in shearography involves the use of a Mach–Zehnder shearing interferometer [77–80]. The principle of the technique is discussed with the help of figure 15. A typical Mach–Zehnder shearing interferometer composed of two mirrors M1 and M2 and beamsplitters B1 and B2 is shown in figure 15(*a*). The lengths of the interferometer arms are exaggerated here for the clarity of demonstration. The magnitude of the Fourier transform of a sheared interferogram recorded with this arrangement is shown in figure 15(*b*). The central values have been deleted to show the spectrum clearly in a scaled image. Reducing the aperture of an iris located at the front

[3] Designed by R M Groves and R P Tatam. Discussed on p102 of [76].

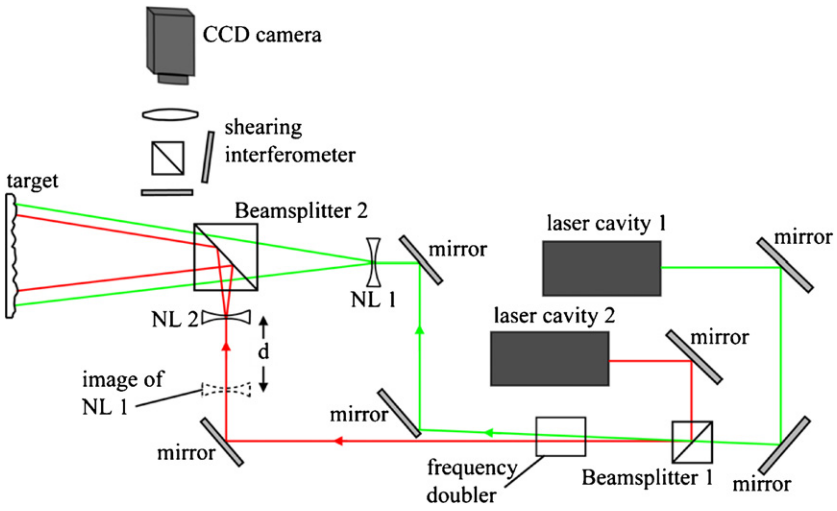


**Figure 14.** Carrier frequency generation in dual-pulsed shearography based on the source translation approach [75].

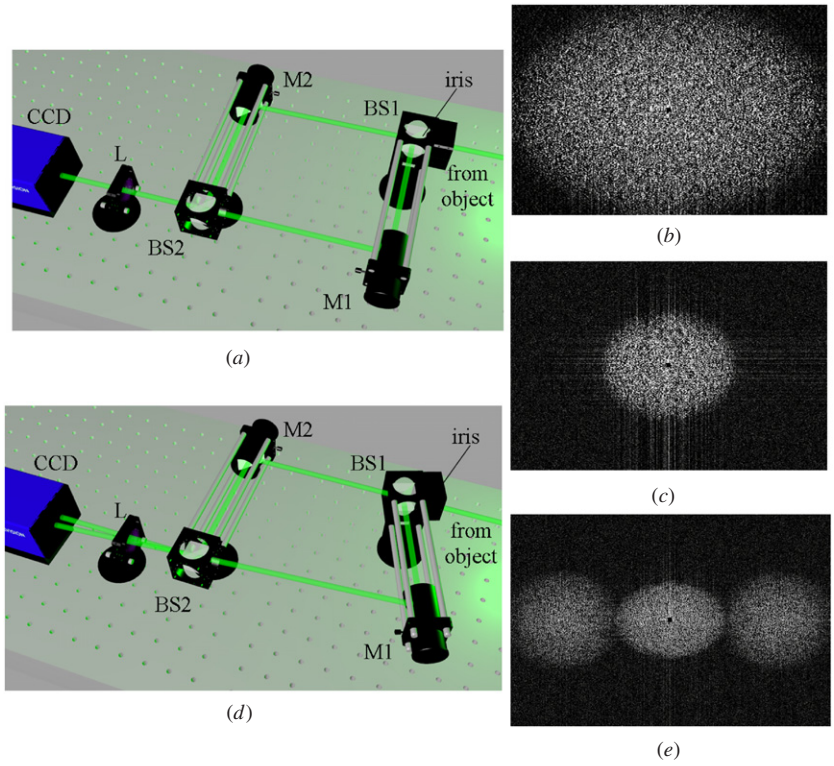


**Figure 15.** A Mach–Zehnder shearing interferometer with parallel arms (*a*) and the Fourier transform of the recorded intensity distribution with a large circular aperture (*b*). Reducing the aperture diameter reduces the dimensions of the spectral feature (*c*). Applying a tilt between the two arms of the interferometer (*d*) introduces the carrier frequency and separates the phase-dependent terms from the background term in frequency space (*e*). $L$ = imaging lens, $M$ = mirror and BS = beamsplitter.

of the interferometer reduces the size of the spectral feature in frequency space as shown in figure 15(*c*). This is because the intensity recorded by the camera is the Fourier transform of the aperture function due to the imaging lens $L$. This also has the effect of increasing the size of the speckles in the recorded speckle pattern. Introducing a tilt between the two interferometer arms, as shown in figure 15(*d*), introduces a phase variation between the interfering wavefronts, resulting in a carrier frequency being introduced into the recorded speckle pattern. Alternatively, the carrier frequency can be introduced by translating one of the mirrors [78]. The phase-dependent terms will then be separated from the background in frequency space, as shown in figure 15(*e*). The carrier fringe pattern generated with this method is much higher frequency than those generated with the source translation technique, with only 2–3 pixels per carrier fringe. The average speckle size needs to be at least twice the size of a carrier fringe in order to be adequately sampled. A speckle pattern containing a carrier frequency is shown in figure 16(*a*). A region within the speckle pattern is enlarged to clearly demonstrate the carrier fringes

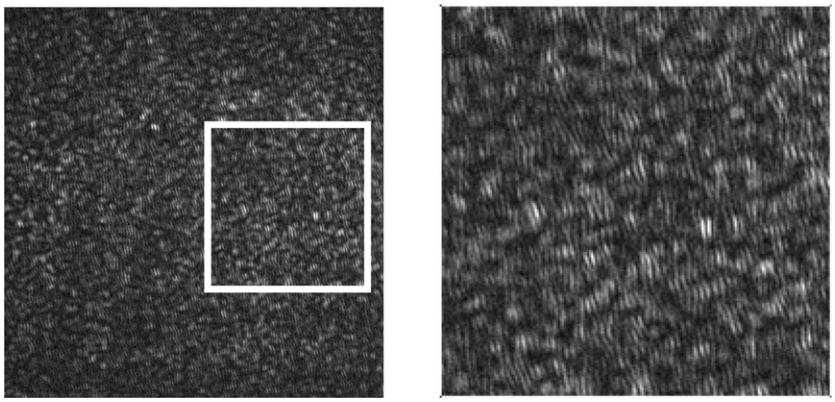

(*a*) (*b*)

**Figure 16.** A sheared speckle pattern with a carrier frequency introduced (*a*). The region within the white box is magnified to show clearly the carrier fringes (*b*) [79].

in figure 16(*b*). One of the drawbacks with this technique is that the light efficiency is quite low due to the relatively small aperture at the input of the interferometer. This may not be too problematic however if a powerful pulsed laser is used.

An alternative processing method, if the carrier frequency is known, involves calculating the phase from neighbouring pixels using a phase-stepping algorithm, such as those given in equations (21) and (22). This has been demonstrated using a double-aperture shearography system [81]. Beams passing through the two apertures exit with a relative tilt between them resulting in a carrier frequency that is observed across the speckles, similar to that shown in figure 16(*b*).

### *4.4. Single fringe pattern demodulation*

An alternative to carrier fringe methods is to calculate the phase from a single fringe pattern. A range of techniques exist to do this but they can be quite complex and computationally intensive. One method, known as skeletonizing, involves thinning the fringes so that they are 1 pixel thick. An image is then produced where +1 or −1 is recorded for maxima and minima respectively and 0 for all other points [82]. The phase between the skeletons is then determined by interpolation. The difficulty lies in accurate determination of the fringe peaks and troughs whilst ensuring that there are no breaks in the fringe skeletons. With speckle correlation fringes there is a lot of high frequency noise so extensive filtering is required.

The windowed Fourier transform has also been used in the determination of phase. One technique known as windowed Fourier ridges (WFR) [83] involves interrogating small regions of the fringe pattern and comparing the spatial frequencies with the windowed transform spectrum. The spatial frequency values with the greatest similarity, known as the ridge, are taken as the local frequencies, which are related to the phase derivatives. The phase can then be calculated from the local frequency values either by integration or from the arctangent of the ratio of real to imaginary parts. Figure 17 shows the demodulated phase of some simulated fringe patterns using the WFR technique. This was done using code given in [83]. Note with the closed fringe pattern on the right of the figure errors

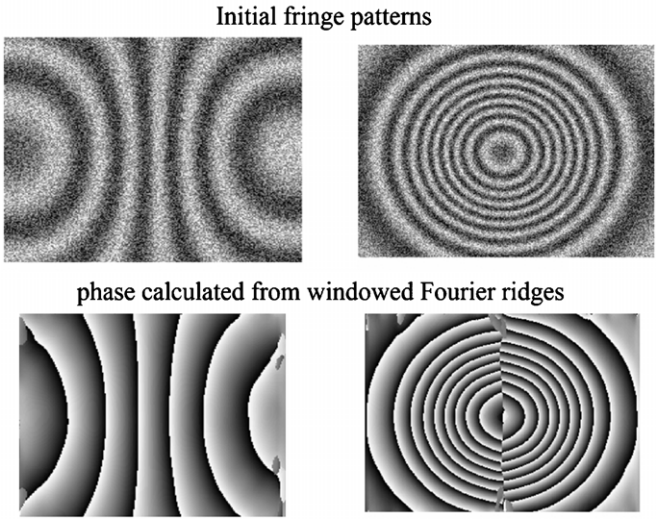


**Figure 17.** Phase demodulation from single fringe patterns using the windowed Fourier ridges technique. Images generated with Matlab® using code presented in [83].

due to sign ambiguities manifest as a discontinuity running vertically through the phase map.

A similar approach is the frequency-guided sequential demodulation technique [84]. In this approach the fringe pattern is first filtered and then normalized using a Hilbert transform. The phase is then estimated by taking the cosine of the pre-processed fringe pattern and the local frequencies are then determined by finding the frequency values that minimize a cost function based on the initial estimate within a small neighbourhood of pixels. The signs of the local frequencies and the phase at each pixel are then determined in sequence dependent on the highest total frequency values of each pixel. This method has been shown to work even with closed fringe patterns.

The continuous wavelet transformation has also been used to determine the phase from single shearography fringe patterns [46, 85]. This can be used in the analysis of continuous deformation with images obtained by a high-speed camera (60 frames per second in [85]). The intensity variation at each

pixel is determined and a temporal wavelet transformation is applied. The 1D temporal intensity variation is converted to a 2D plane, the maxima of which (the ridge) correspond to the local frequency. The phase can then be determined from the arctangent of imaginary to real parts of the ridge frequencies. One advantage of the wavelet transformation is that the demodulated phase is obtained unwrapped, so there is no need for a post-process unwrapping algorithm (section 4.5).

All the techniques discussed in this section are suitable for phase demodulation from a single fringe pattern however they can be rather computationally complex and intensive and would therefore not be suitable for live phase map generation. For instance the windowed Fourier ridges takes 3 min to demodulate a 256 × 256 image using Matlab® code on a Pentium IV 3.2 GHz PC [83]. For shearography, the factors contributing to choice of technique would include its resilience to noise and whether or not closed fringe patterns are likely to be generated.

### *4.5. Filtering*

Speckle interferometry techniques by their very nature are subject to significant levels of high frequency noise. Filtering is often used to reduce the high frequency noise prior to further image processing steps such as phase unwrapping. The typical method of removing high frequency noise is to apply a low-pass filter. This is done through the 2D convolution of the image with a low-pass filter kernel. The simplest low-pass filter kernel is the 3 × 3 kernel:

$$K_{\text{low-pass}} = \frac{1}{9}\begin{bmatrix} 1 & 1 & 1 \\ 1 & 1 & 1 \\ 1 & 1 & 1 \end{bmatrix} \tag{28}$$

This returns the value of a particular pixel as the average of values within a 3 × 3 neighbourhood centred on the pixel and results in blurring or smoothing of an image.

When filtering wrapped phase maps often the sine and cosine are determined to which a low pass filter is applied. The filtered wrapped phase map is then obtained from the sine and cosine maps using an arctan function. The filtering effect can be increased either by applying the filter multiple times or by using a filter kernel with larger dimensions. The danger with over-filtering, however, is that the phase fringe discontinuities will be blurred out. Aebischer and Waldner [86] suggest applying a small filter kernel numerous times, but with an intermediate phase recalculation after each filter pass. This effectively removes noise from the phase map without blurring out the phase fringe discontinuities. Figure 18 shows a comparison between processing a simulated phase map with a 19 × 19 low pass filter kernel, a 3 × 3 kernel 30 times and a 3 × 3 kernel 30 times but with an intermediate phase calculation between each filter pass. The latter shows no degradation of the phase fringes at the centre of the image unlike the two former examples.

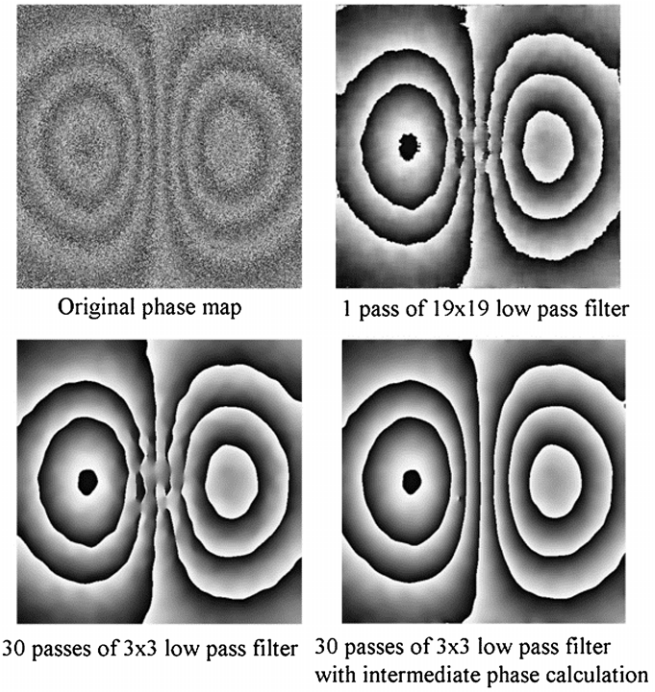


**Figure 18.** Comparison of some basic low-pass filtering schemes for removing high frequency noise from wrapped phase maps.

### *4.6. Phase unwrapping*

Wrapped phase maps are bound between $-\pi$ and $+\pi$. To obtain a continuous phase measurement these $2\pi$ discontinuities need to be removed. This process is known as phase unwrapping. A typical wrapped phase map is shown in figure 19(*a*) and a plot along a line horizontally through the centre of the wrapped phase map is shown in figure 19(*b*) where the discontinuities can clearly be seen when the phase passes $-\pi$ or $+\pi$. Figures 19(*c*) and (*d*) show the result after phase unwrapping with the $2\pi$ fringe discontinuities removed.

In the case of the phase map shown in figure 19(*a*), phase unwrapping can be performed by simply scanning along each row and adding or subtracting $2\pi$ whenever the phase passes $-\pi$ or $+\pi$, respectively. In practical shearography, however, the phase maps are often subject to high frequency noise or there may be breaks in the wrapped phase fringes or other difficulties such as holes in the object may exist. Therefore more sophisticated unwrapping procedures are often required.

A popular unwrapping algorithm is the branch cut algorithm [87]. This algorithm involves the detection of phase residues which are found at the points where the breaks in the fringes occur. The residues are assigned either positive or negative values depending on the sum of the phase values of neighbouring pixels. The next step is to place branch cuts which connect positive and negative residues. The phase is then unwrapped pixel-by-pixel avoiding the branch cuts producing an unwrapped phase map.

Another approach involves unwrapping pixels in order of quality. The quality is determined from the phase gradients within the phase map. The phase is unwrapped along the path of the minimum spanning tree [88]. In a weighted

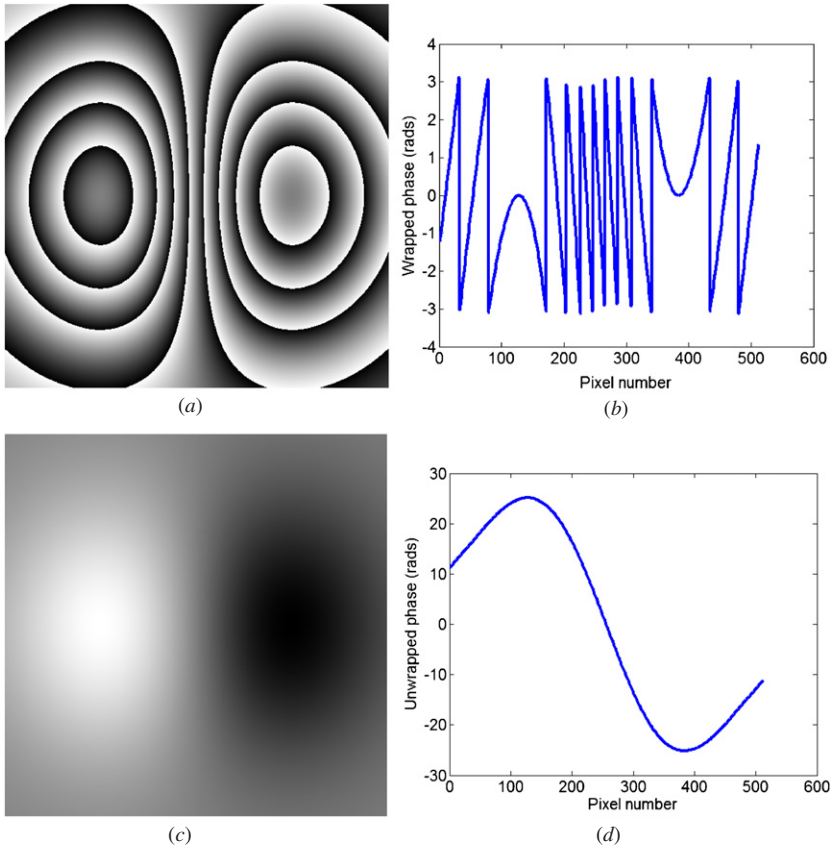


**Figure 19.** Wrapped (*a*) and unwrapped (*c*) phase maps with a plot along a line through the centre of the wrapped (*b*) and unwrapped (*d*) maps.

graph the minimum spanning tree is a connecting tree that connects all vertices with the minimum total weight. In phase unwrapping, the speed of the process can be improved by considering smaller regions of data within the phase map known as tiles [89]. A recent publication describes the application of a regional phase unwrapping algorithm based on fringe estimation and phase map segmentation to wrapped phase maps generated using speckle interferometry [90].

The branch cut algorithm has been extended to three dimensions [91]. It has been discovered that the phase residues create loops in three-dimensional space. The technique is useful in magnetic resonance imaging, which produces three-dimensional data, but can also be useful in high-speed shearography when sequences of phase measurements are made. The book by Ghiglia and Pritt [11] contains detailed descriptions of a number of phase unwrapping algorithms along with C code implementations of each of them.

A number of commercial software packages offer phase unwrapping among other functions. Some examples are ISTRA from Dantec Dynamics [92], OPTOCAT from Breukmann GmbH [93] and isi-studio (Shearwin NT) from Isi-Sys [94].

### *4.7. Errors and uncertainties*

In this section some of the sources of error in shearography measurements are discussed.

*4.7.1. Errors associated with shear amount.* One error source is due to the assumption that it is displacement derivative that is being measured when in fact shearography measures displacement differences between points separated by the shear distance. This assumption leads to the exclusion of higher order displacement derivative terms in the derivation of equation (10). The higher order terms are present within the shearography measurement and increase uncertainty in a measurement of first-order displacement derivative. This uncertainty can be reduced by minimizing the image shear at the cost of measurement sensitivity. Techniques have also been presented which remove the image doubling effect and reconstruct the displacement field. This can be done by summing phase values along a row of pixels over the shear distance [95] or by using Fourier transform techniques [96]. The displacement derivatives can then be obtained through numerical differentiation, although this will introduce errors associated with the numerical differentiation process. However, the techniques can be used as an alternative to ESPI with the advantage of retaining the inherent stability of shearography. A recent publication discusses in detail the implications of the shear magnitude in Michelson interferometer-based shearography measurements [97]. Different techniques for calculating the displacement gradient for non-planar surfaces are discussed in detail in [98].

*4.7.2. Errors associated with configuration of multiple measurement channels.* Another source of error that occurs

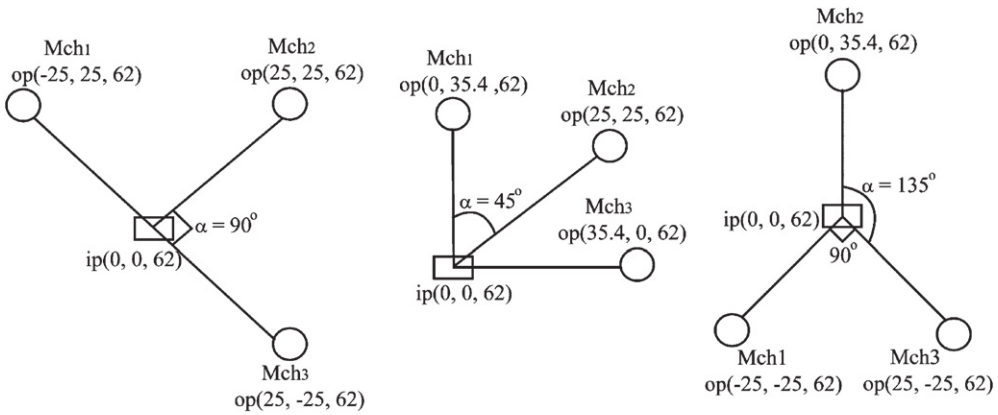


**Figure 20.** Some different possibilities for multi-component viewing configurations and the associated condition numbers. Mch = measurement channel, op = observation position and ip = illumination position.

in multi-component strain measurements is due to the use of a matrix transformation to convert from the non-orthogonal measurements to resolve the orthogonal displacement derivative components. The level of uncertainty associated with a matrix operation can be roughly characterized by its condition number. Reducing this number effectively reduces the errors associated with the operation. It has been shown that the condition number of the transformation matrix is dependent on the illumination or observation configuration [99]. Figure 20 shows some example multiple observation direction configurations with different angular separations $\alpha$ between the three measurement channels. The working distance is kept fixed at 62 cm and the observation angle is also fixed at 30°. The coordinate locations of the observation positions (op) and the illumination position (ip) are given in the form $(x, y, z)$. The matrix condition number for each configuration was calculated using the Matlab® function cond($M_k$), where $M_k$ is the sensitivity matrix given in equation (15).

The variation of the condition number against angular separation is shown in figure 21(*a*) [76]. The red bars labeled configuration 1–3 mark the locations of the three configurations shown in figure 20. The graph shows that the optimum configuration in terms of minimizing the condition number is when the measurement channels are equi-spaced, although configurations 1 and 3 show similarly low condition numbers. The working distance and observation angles of the configuration also have an influence on the condition number. Figures 21(*b*) and (*c*) show the effect of condition number against the working distance and the observation angle, respectively. In conclusion, the configuration that minimizes the condition number has equi-spaced measurement channels, a short working distance and large observation angles. For multiple-illumination-direction configurations the calculations would be equivalent. This may not be appropriate in a practical shearography system; however a condition number below 20 is considered to be adequate for most measurement applications [99].

*4.7.3. Errors associated with measurement of shear magnitude.* Another significant source of uncertainty in shearography comes from the measurement of shear magnitude. Accurate measurement of the shear magnitude is required to obtain the displacement derivative; however there is little in the literature that describes effective methods of achieving this. Often a single measurement is made at the centre of the image and the shear is then assumed to be constant at each point in the image. One shear measurement technique that has been discussed is digital image correlation/speckle photography [100, 101]. In the speckle photography approach, an image is recorded first with one arm of the interferometer blocked and then the other. The digital cross-correlation is calculated and the shift of the speckle pattern between the images can be obtained from the separation of the correlation peak from the centre of the resultant image. The shear magnitude is related to the shift in the speckle pattern multiplied by the magnification factor of the imaging system. Cross-correlation calculations can be made at different regions of the image to obtain a full-field measurement of the shear magnitude.

*4.7.4. General sources of error in shearography.* A recent study [102] investigated the uncertainties present in shearography due to wavefront divergence with particular consideration paid to the aperture of the imaging system. Both collimated and non-collimated illuminations were considered. It was discovered that at short working distances (∼200 mm) significant phase errors were introduced but quickly reduced to tolerable levels with increasing working distance. Cordero and Labbe [103] used Monte Carlo simulations to quantify errors of in-plane displacement derivative measurements made with shearography. The simulation was conducted by measuring the displacement derivative ∼1000 times using different input parameters generated from the assigned probability density functions. The study found that the measurement uncertainty was greatest at the edges of the illuminated area and where the magnitude of the surface displacement was greatest.

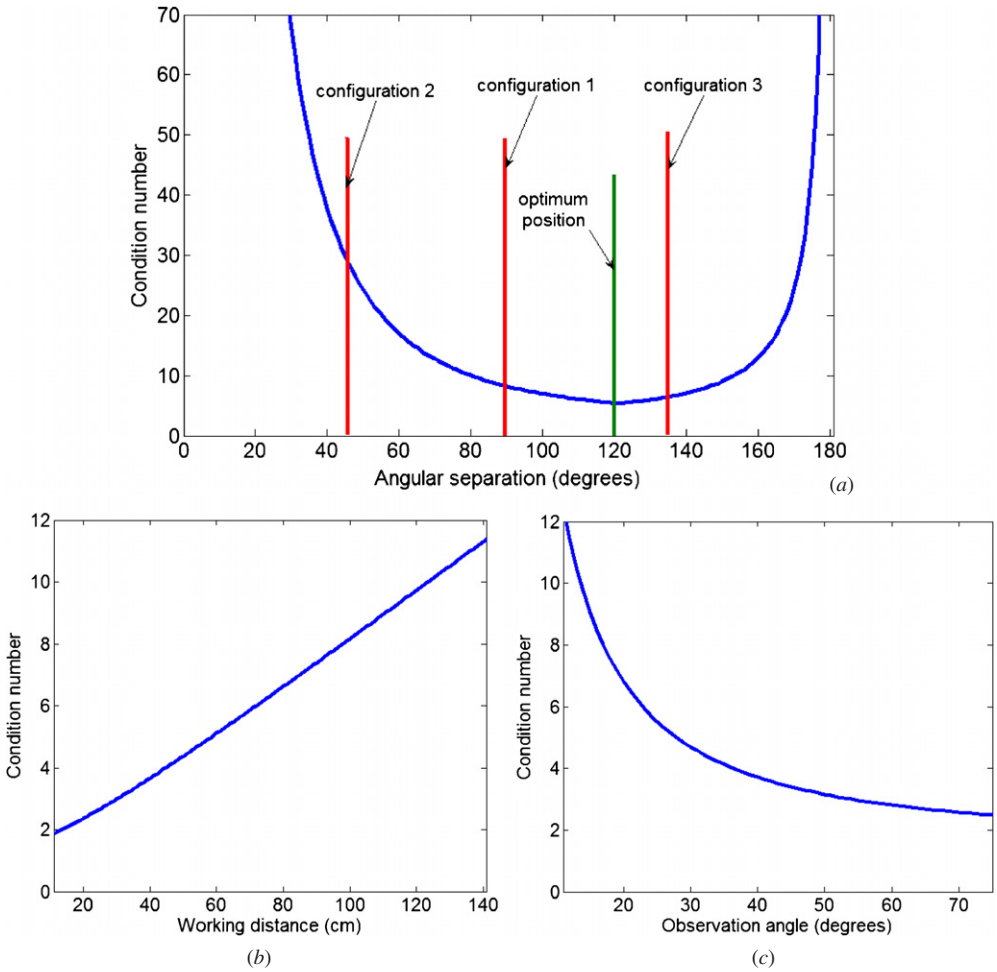


**Figure 21.** The effect of angular separation (*a*), working distance (*b*) and observation angle (*c*) on the condition number of the sensitivity matrix used in the coordinate transformation in multi-component shearography measurements.

## 5. Applications of shearography

### *5.1. Qualitative non-destructive testing*

Shearography has been developed into an important technique in non-destructive testing (NDT) due to its ability to provide a non-contact, full-field measurement. Furthermore, it has a number of advantages over the related techniques of holography and ESPI in that it directly measures the derivative of displacement and it has reduced coherence requirements and sensitivity to vibration due to its use of an almost common-path interferometer. Since shearography directly measures strain anomalies in the region of defects, the successful application of shearography for NDT is dependent on the size and location of the defects, the magnitude of the loading and the magnitude and direction of the shear direction [104].

A common NDT application of shearography is in the aerospace industry [105] where it is used for analysis of structural integrity. Composite panels are frequently used in the aerospace industry because of their high strength to weight ratio. However, they can be subject to delaminations due to impact or shock which can lead to failure of the component. The location of the delaminations and defects can be difficult to determine by eye therefore non-destructive testing is essential in predicting failures. When the component is subject to an applied load, a delaminated regions will exhibit strain anomalies compared with regions that are well adhered. Using shearography the defected regions become visible in the fringe pattern even if they are below the surface since they still have an influence on the surface deformation. Common loading techniques include thermal loading, for example by using high power flash lamps [106], pressure loading by inducing a vacuum [107] around the region of interest or by vibrational excitation [107]. A number of publications have discussed the use of shearography in the non-destructive evaluation of composites, for example [8, 108]. Other papers have compared the use of shearography for composite NDT with other established NDT techniques such as thermography [109, 110] and ultrasonic C-scan [111]. All these applications utilize single-component shearography systems for qualitative inspection.

Figure 22 shows an example of an investigation of an aeroplane panel that experienced damage due to a hailstorm [112]. The measurements were made with a single-component, out-of-plane displacement gradient-sensitive shearography system. The aeroplane and the panel under investigation are shown in figures 22(*a*) and (*b*), respectively. A region of the surface of the panel with an

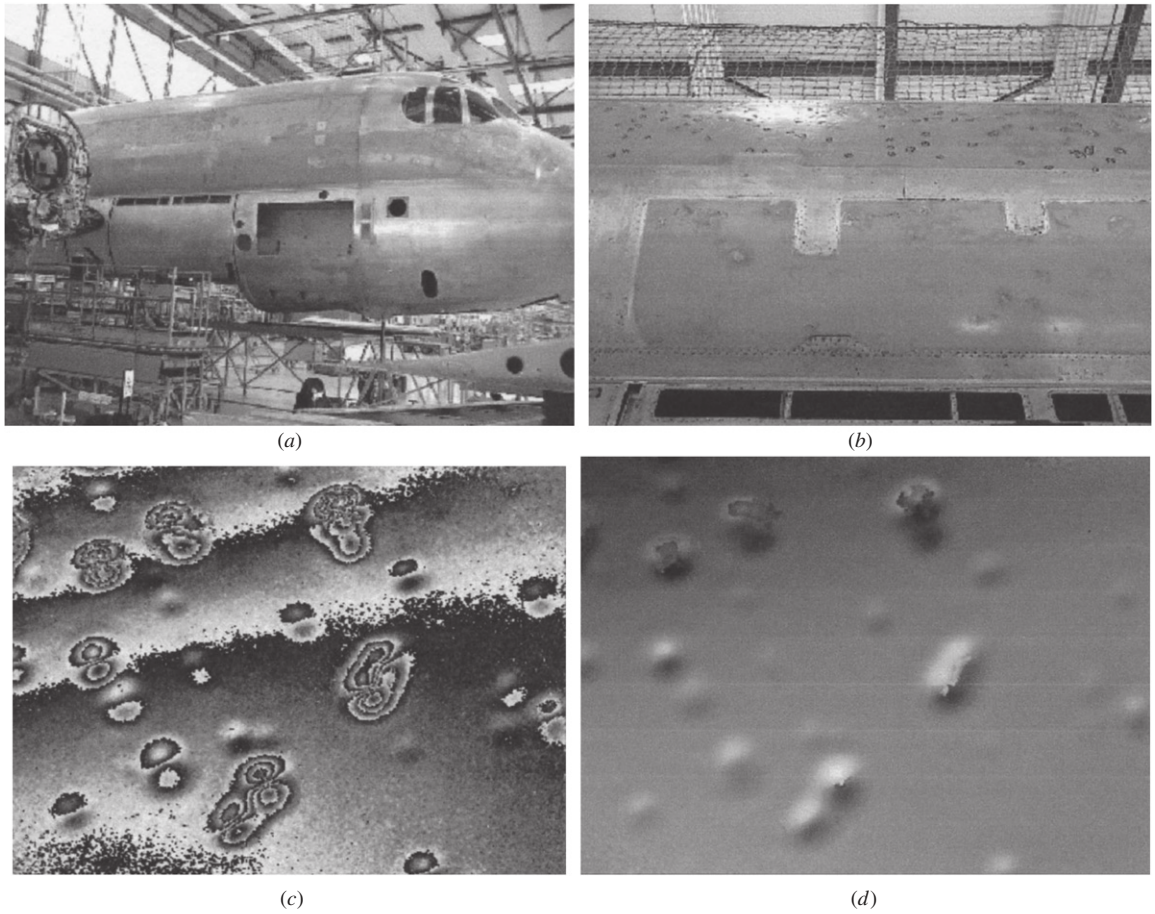

**Figure 22.** Shearography investigation of a hailstorm-damaged aeroplane body. The plane and area under test are shown in (*a*) and (*b*). The wrapped and unwrapped phase maps are shown in (*c*) and (*d*) [112].

area of approximately 50 cm$^2$ was loaded thermally using an infrared source. The processed wrapped phase map is shown in figure 22(*c*) and the unwrapped phase map is shown in figure 22(*d*). The damage locations can clearly be seen in the shearography results.

One example of a composite panel is the GLARE (GLAss REinforced) panel, developed in the Faculty of Aerospace Engineering, Delft University of Technology, which was used in the manufacture of the fuselage of the Airbus A380. It consists of alternating bonded layers of thin aluminium alloy sheets and glass fibre pre-preg. Figure 23 shows results of an investigation of a GLARE panel using shearography with nine pre-prepared delaminations between the aluminium sheets of 60 mm diameter within it [113]. The locations of the defects are indicated by the circles in the figure. Image processing is used here to reveal the defects and not to provide quantitative information.

Other related investigations using shearography that have been reported in recent publications include the identification of defects in GRID-LOCK® joints [114] and analysis of strain distributions around the inserts in composite plates [115]. GRID-LOCK® is a novel method of joining structural components that was developed by the Goodrich Corporation and used recently in the F-15E fighter aircraft. Inserts are used in composite sandwich plates to transmit loads. Shearography is also used in the rubber industry for the non-destructive inspection of tyres to detect delaminations along a steel belt on the interior of the tyre [116]. Santos *et al* [78] used a pulsed ruby laser to investigate shock waves propagating through composite panels. A Mach–Zehnder shearing interferometer was used in conjunction with the temporal carrier technique to obtain wrapped phase maps, as discussed in section 4.3. Recently, Lamb waves in composite fibre reinforced plastics (CFRP) have been investigated using pulsed laser shearography using a Mach–Zehnder shearing interferometer to generate a spatial carrier [79].

Another example of an application of NDT is in the preservation of artworks. A recent publication [117] describes the use of shearography and terahertz imaging to evaluate a wooden panel painting. Shearography was used to investigate surface and sub-surface defects, whereas terahertz imaging can be used to obtain defect information throughout the depth of the sample. An artificial sample was constructed in the style of a mediaeval Greek painting and analyzed using shearography and terahertz imaging. The size of the sample was 201 mm wide, 112 mm high and 14 mm thick. The artificial painting and the field of the shearography instrument are shown in figure 24(*a*). The object was loaded thermally using high power infra-red lamps. Figure 24(*b*) shows the unwrapped phase map obtained with loading applied to the rear of the

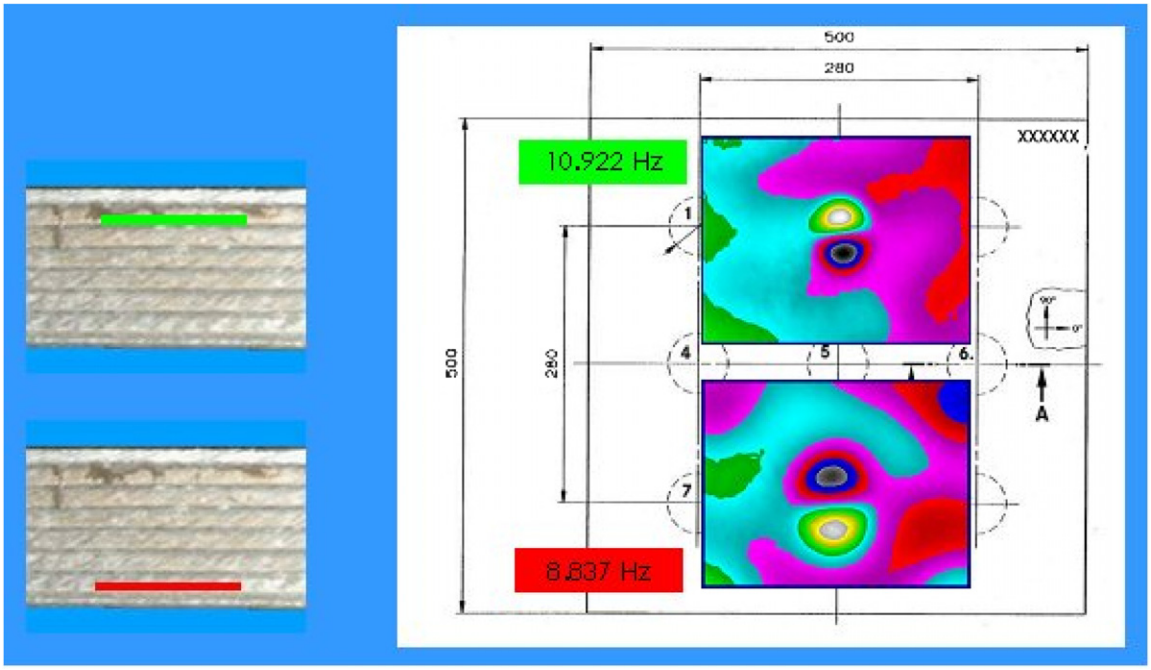


**Figure 23.** Investigation of defects in a GLARE panel. Nine pre-prepared defects at different depths were introduced, as indicated by the circles. Phase measurements were made with vibrational excitation frequencies of 10.922 kHz and 8.837 kHz [113]. The field of view of the two phase maps is approximately 200 × 250 mm$^2$.

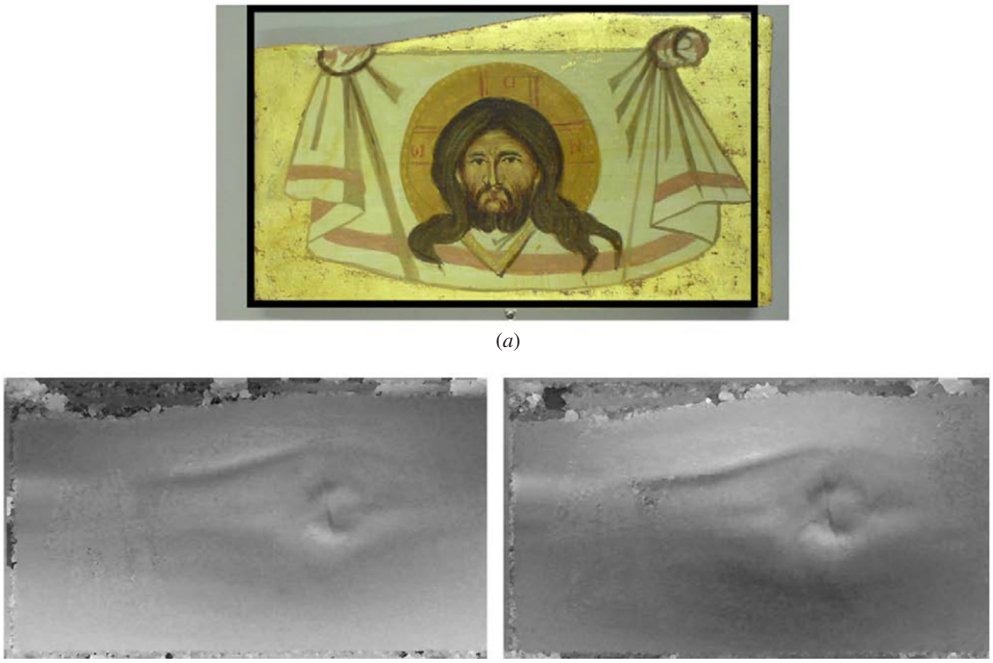

(*a*)

(*b*) (*c*)

**Figure 24.** Analysis of a painting using shearography [117]. The black box in (*a*) indicates the field of view of the instrument, which is approximately 200 mm × 110 mm. Unwrapped phase maps obtained with thermal loading applied to the rear and the front of the painting are shown in (*b*) and (*c*) respectively.

object and figure 24(*c*) shows the unwrapped phase when the front of object was thermally loaded. The results clearly show the presence of a knot in the wood. The discontinuity in the centre of the knot is due to a small crack in the paint layer. One of the difficulties that were encountered during the measurements was due to the different surface reflectivities. In regions where the reflectivity was low, there was low modulation therefore poor measurement quality in these areas. To address this issue, an extended dynamic range technique for shearography, based on that used in photography, was developed [59]. This technique involved recording each image twice but with different exposures. The images are

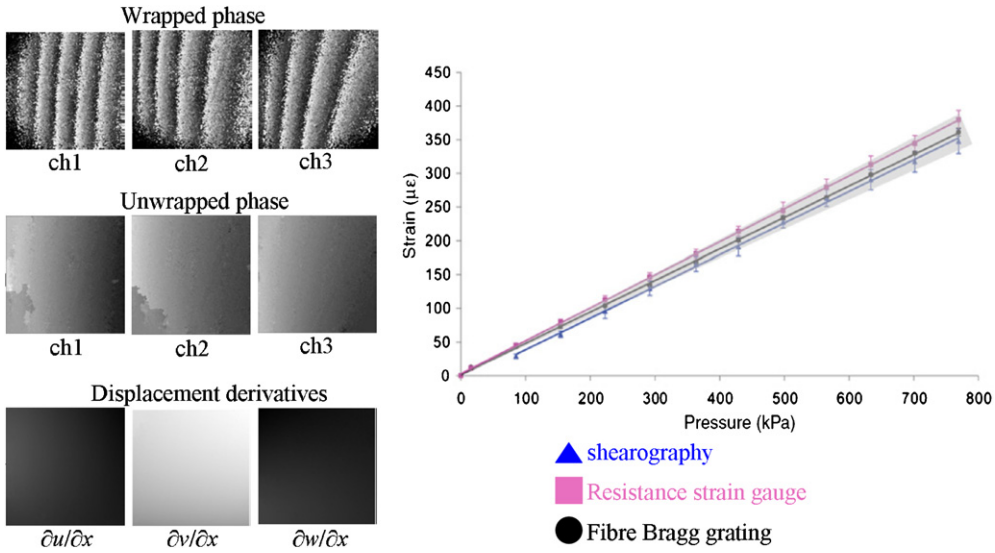


**Figure 25.** Results of a multi-component shearography measurement of a hydrostatically loaded pipe showing the wrapped and unwrapped phase maps and the calculated displacement derivatives. The graph shows the measured strain using shearography, a resistance strain gauge and a fibre Bragg grating. The shaded region indicates the standard deviation of a theoretical calculation [9].

then combined resulting in an image with improved dynamic range and therefore improved measurement quality in regions of previously low modulation.

### *5.2. Applications of quantitative strain measurement in shearography*

Shearography has been used to determine the strain around welds. Steinchen *et al* [118] used shearography to measure surface strain around welded aluminium samples. The samples were loaded using a tensile test machine. The shearography instrument employed a configuration with four laser diodes and two shearing interferometers and cameras. The four in-plane strain components were measured using pairs of beams in either the $x$–$z$ or $y$–$z$ planes and the two out-of-plane strain components where measured using a single beam. The use of two shearing interferometers allowed the measurement of all six strain components in a single loading step.

Groves *et al* [119] report surface strain measurements from a pipe in the region of a weld. Since the pipe was cylindrical, a correction was required because of the variation in shear and sensitivity vector due to the shape of the object. This was achieved using the source displacement technique discussed in section 3.2. The pipe was hydrostatically loaded before the reference frames were captured and then depressurized before the signal frames were recorded. Strain measurements from a hydrostatically loaded cylindrical pipe have been quantitatively compared with measurements obtained using resistance strain gauges and fibre Bragg grating instrumentation [9]. Some of the results of this investigation are shown in figure 25. The wrapped and unwrapped phase maps obtained from each of the three measurement channels (ch1–ch3) are shown as well as the calculated displacement derivatives. The graph shows the measured strain versus pressure for the three techniques, all of which lie within the standard deviation of the theoretical calculation indicated by the shaded area.

Another application of quantitative shearography was in the measurement of strain distributions around cracks [120]. Figure 26 shows the results of measurements of a titanium alloy comprising vanadium, iron and aluminium. A 3 mm radius notch was located on one side of the sample and the crack was located adjacent to the notch. The measurements shown were obtained through incremental loading from 1 kN to 10 kN in a tensile test machine. Phase measurements made at each loading step (200 N) were summed to derive the final measurement. The loading step was carefully chosen to prevent $2\pi$ phase wrapping, therefore no additional phase unwrapping was required. The samples were then applied with a polymeric coating to simulate a practical component and the measurements were repeated. The result of the coating was that a larger tensile stress was required in order to detect the crack.

A recent publication describes the use of shearography for surface strain measurement of rotating objects [79]. This was done using a pulsed Nd:YAG laser and four observation directions to produce the different measurement sensitivities. This was realized using four camera lenses which were connected to a four-arm fibre-optic imaging bundle. Light exiting the fibre-bundle distal end was imaged onto a CCD camera through a Mach–Zehnder interferometer which served to introduce image shear and a carrier frequency. The arrangement of this system is shown in figure 27. The object that was investigated was a PTFE plate with an aluminium disk embedded in it. The object, mounted on a lathe, was thermally loaded and set to rotate at a frequency close to the 10 Hz nominal repetition rate of the laser. The laser was then triggered on each rotation of the lathe.

Images were recorded as the object cooled and phase measurements were made from two recordings using the spatial carrier technique discussed in section 4.3. Multi-component surface strain measurements were obtained from unwrapped phase maps using a matrix transformation based on

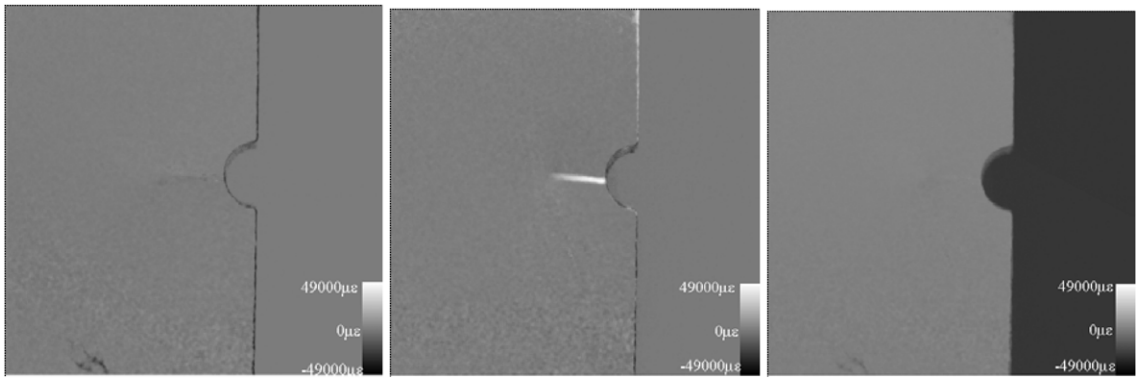


(*a*) (*b*) (*c*)

**Figure 26.** Surface strain measurement of a titanium 10-2-3 alloy containing a fatigue crack. The surface strains shown are $\partial u/\partial y$ (*a*), $\partial v/\partial y$ (*b*) and $\partial w/\partial y$ (*c*) [120].

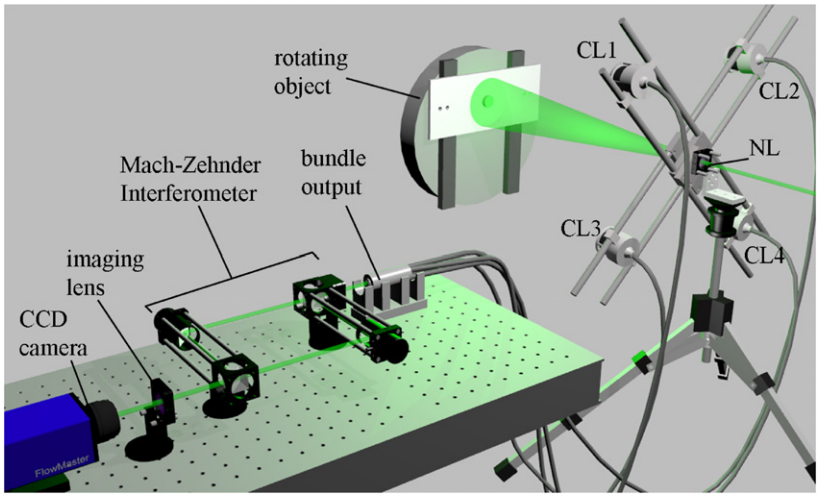


**Figure 27.** Experimental arrangement of a multi-component, pulsed laser shearography system used for quantitative surface strain measurement on rotating objects [79]. CL1–4 represent the four camera lenses and NL is a negative lens used to diverge the laser light.

measurements of the observation and illumination positions. Figure 28 shows the orthogonal displacement derivative components calculated from unwrapped phase maps produced with the shearography system. The strain was observed to be predominantly out-of-plane with greatest variation around the periphery of the aluminium disk. This was expected considering the nature of the loading and the strain values obtained compared well with a theoretical calculation based on the thermal expansion coefficients of the materials involved and the temperature variation.

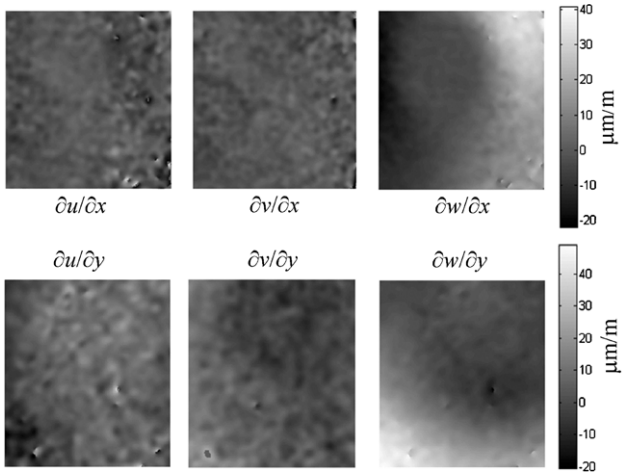


**Figure 28.** Orthogonal displacement derivatives calculated from unwrapped phase maps generated using the shearography system shown in figure 27. The field of view is approximately 40 mm × 35 mm [79].

### *5.3. Small-scale measurements*

A number of recent publications have reported some interesting applications of shearography for investigation of objects over a small field of view. This is of particular importance in the electronics industry where stress characterization of components is required to determine their reliability. Dilhaire *et al* [121] describe a shearography system based on a Wollaston prism that was used to measure surface displacement derivatives of a MOS (metal oxide semiconductor) transistor with dimensions approximately 5 mm$^2$. The transistor was calibrated while it was switched off, then with the power switched on measurements were made. Thermal effects induced surface bending which was measured with shearography.

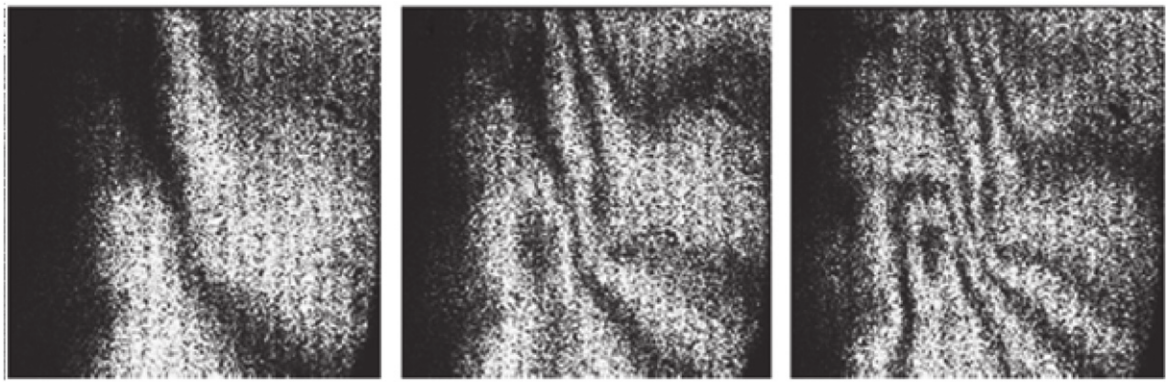

(*a*) (*b*) (*c*)

**Figure 29.** Correlation fringe patterns obtained using shearography from an amorphous material 30s (*a*), 33s (*b*) and 36s (*c*) after deformation. The images were recorded with a field of view of 2 mm$^2$ [123].

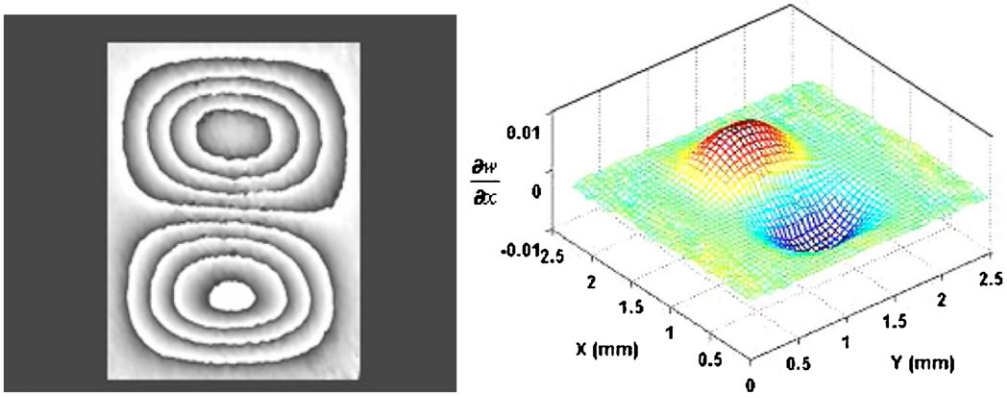


(*a*) (*b*)

**Figure 30.** Wrapped phase map (*a*) and displacement derivative measurement (*b*) from a MEMS pressure sensor. The field of view is 2.5 mm$^2$ [124].

Udupa *et al* [122] describe the use of shearography for the detection of defects in unpolished silicon wafers used in the semiconductor industry. Conventionally, in the manufacturing process, batches of wafers are polished before being assessed for defects. Therefore the rejected wafers undergo unnecessary polishing which wastes time and money. A 200 mm diameter wafer was investigated for defects by thermally loading the sample with an infrared lamp. Shearography was able to successfully detect defects ranging in size from 2 to 20 mm. With further adjustments of the imaging optics, defect diameters of approximately 100 $\mu$m are predicted to be detectable.

MEMS (microelectromechanical systems) are microscopic machines consisting of components ranging from 1 to 100 $\mu$m and are used as sensors and actuators. Knowledge of their response to external loads is important in the assessment of their reliability. A couple of very recent publications have described the use of shearography in MEMS characterization. Mihaylova and Toal [123] report the use of a simple shearing interferometer based on a pair of glass plates (shown in figure 9(*a*)) that is suitable for MEMS measurements. A long working distance microscope objective was used as the imaging lens and correlation fringes were demonstrated using a flexible amorphous material over a field of view of 2 mm$^2$, as shown in figure 29. Phase shifting using the interferometer was also demonstrated in a macroscopic configuration.

Kumar *et al* [124] describe the analysis of a MEMS device using a conventional Michelson shearing interferometer. A zoom lens module allowed measurements over a field of view of 2.5 mm$^2$. The illumination intensity was controlled using a neutral density filter and an iris which determined the diameter of the illuminated area. Images were recorded before and after an applied pressure of 80 kPa and the phase was recovered using an eight-step algorithm that compensates for phase-shift errors. Figure 30 shows an out-of-plane displacement derivative measurement of a MEMS pressure sensor with dimensions of 1.5 mm$^2$.

Shearography displacement derivative measurements have also been applied to the analysis of tissue phantoms [125]. A comparison of normal specimens with those containing abnormalities showed encouraging results with non-destructive evaluation of living biological samples the subject of future research. A later publication [126] describes


**Figure 31.** Some of the commercial shearography systems that are available on the market; the Q-800 from Dantec Dynamics (*a*) [127], the Steinbichler ISIS mobile 3000 (*b*) [128], the Optonor SNT 4045 (*c*) [129] and the SE3-NDT from ISI-sys (*d*) [130].

the incorporation of an endoscope with ESPI and shearography for intra-intestinal inspection.

### *5.4. Commercial systems*

A number of companies supply shearography systems. One of the leading suppliers of laser-based measurement systems is Dantec Dynamics [127], based in Germany. They manufacture, among others, the Q-800 portable shearography system for NDT, shown in figure 31(*a*). The system consists of four diode lasers, a miniaturized Michelson shearing interferometer and a 1392 × 1040 pixel array CCD camera. This compact system can be easily mounted on a tripod for a range of measurement applications. Another company that specializes in commercial shearography systems is Steinbichler Optotechnik GmbH [128]. The ISIS mobile 3000 from Steinbichler is shown in figure 31(*b*). This instrument is compact and easy to use as it can be fixed directly to the object under investigation. The SNT 4045 from Optonor in Norway [129] shown in figure 31(*c*) is another compact tripod mounted shearography system developed for non-destructive testing. This instrument utilizes vibrational excitation to apply dynamic loading to the object under investigation. The SE3-NDT from ISI-sys [130], shown in figure 31(*d*), also employs vibrational excitation for object loading. This is facilitated by a piezo shaker that mounts on to the surface of interest. Other developers of commercial shearography systems include Laser Optical Engineering [131] in Loughborough, UK, and Laser Technology Inc. [132] in the USA. Most of the commercial systems are suitable for qualitative inspection and are not used for quantitative surface strain measurement. This indicates that although successfully demonstrated in the laboratory as a quantitative, full-field surface strain measurement technique, there are still several limitations that need to be overcome before quantitative shearography can be fully commercialized.

## 6. Conclusions and outlook

This review has reviewed the optoelectronic measurement technique shearography and its associated instrumentation, technology and image processing routines. Over the last ten years or so, shearography has evolved into a useful and efficient tool for non-destructive testing. This is due to its inherent resilience to environmental disturbances and its ability to provide a non-contact, full-field measurement. Quantitative surface strain measurement has also been demonstrated in the laboratory using multi-component shearography instrumentation; however it has yet to evolve into an established measurement tool for industrial strain measurement.

Shearography is also suitable for measurement of the object's shape, analysis of vibrational modes as well as measurements of curvature and twist. Coupled with pulsed illumination, shearography has been shown to be suitable for measurement of dynamic and transient loading events. To make quantitative measurements, recovery of the phase variation between recordings is required. Recovery of the phase is also useful in qualitative assessments since phase maps are more easily interpreted than correlation fringe maps. For static loading events this can be achieved using temporal phase-stepping techniques. For dynamic measurements, however, more complex phase analysis procedures such as the frequency-based techniques are required. This is due to the requisite that all necessary data corresponding to signal and reference states need to be acquired instantaneously. Phase maps are usually obtained wrapped within $2\pi$ boundaries. The discontinuities need to be removed in order to obtain a continuous measurement and there are a number phase unwrapping algorithms suitable for this purpose. The number of measurement applications is continually growing. Now, in addition to more traditional applications such as delamination detection in composite materials, many other applications such as evaluation of artworks, assessment of electrical components and even medical applications are being reported.

## Acknowledgments

D F would like to acknowledge a Visiting Research Fellowship at TU Delft. The framework for exchange of researchers was established at the 2009 Workshop in Aerospace Materials, Structures and Sensing at Cranfield University, funded by the British Council, UK, and Platform Bèta Techniek, The Netherlands.

## References

[1] Steinchen W, Yang L X, Kupfer G, Mäckel P and Vössing F 1998 Strain analysis by means of digital shearography: potential, limitations and demonstrations *J. Strain Anal.* **33** 171–82

[2] Pan B, Kemao Q, Xie H and Asundi A 2009 Two-dimensional digital image correlation for in-plane displacement and strain measurement: a review *Meas. Sci. Technol.* **20** 062001

[3] Rao Y J 1999 Recent progress in applications of in-fibre Bragg grating sensors *Opt. Laser. Eng.* **31** 297–324

[4] Leendertz J A and Butters J N 1973 An image-shearing speckle-pattern interferometer for measuring bending moments *J. Phys. E: Sci. Instrum.* **6** 1107–10

[5] Hung Y Y 1982 Shearography: a new optical method for strain measurement and non-destructive testing *Opt. Eng.* **21** 391–5

[6] Hung Y Y 1997 Digital shearography versus TV-holography for non-destructive evaluation *Opt. Laser. Eng.* **26** 421–36

[7] Hung Y Y 1996 Shearography for non-destructive evaluation of composite structures *Opt. Laser. Eng.* **24** 161–82

[8] Hung Y Y 1999 Applications of digital shearography for testing of composite structures *Composites* B **30** 765–73

[9] Groves R M, Chehura E, Li W, Staines S E, James S W and Tatam R P 2007 Surface strain measurement: a comparison of speckle shearing interferometry and optical fibre Bragg gratings with resistance foil strain gauges *Meas. Sci. Technol.* **18** 1175–84

[10] Creath K 1993 Temporal phase measurement methods *Interferogram Analysis, Digital Fringe Pattern Measurement Techniques* ed D W Robinson and G T Reid (Bristol: Institute of Physics Publishing)

[11] Ghiglia D C and Pritt M D 1998 *Two-Dimensional Phase Unwrapping: Theory, Algorithms and Software* (Chichester: Wiley)

[12] Francis D, James S W and Tatam R P 2007 Surface strain measurement using multi-component shearography with coherent fibre-optic imaging bundles *Meas. Sci. Technol.* **18** 3583–91

[13] Hung Y Y and Liang C Y 1979 Image shearing camera for direct measurement of surface strains *Appl. Opt.* **18** 1046–51

[14] Gan Y and Steinchen W 2008 Speckle methods *Springer Handbook of Experimental Solid Mechanics* ed W N Sharpe (New York: Springer)

[15] Steinchen W and Yang L X 2003 *Digital Shearography* (Bellingham, WA: SPIE)

[16] Hung Y Y and Wang J Q 1996 Dual-beam phase shift shearography for measurement of in-plane strains *Opt. Laser. Eng.* **24** 403–13

[17] Steinchen W, Yang L X and Schuth M 1996 TV-shearography for measuring 3D-strains *Strain* **32** 49–57

[18] James S W and Tatam R P 1999 Time-division-multiplexed 3D shearography *Proc. SPIE* **3744** 394–403

[19] Waldner S and Brem S 1999 Compact shearography system for the measurement of 3D deformation *Proc. SPIE* **3745** 141–7

[20] Kästle R, Hack E and Sennhauser U 1999 Multiwavelength shearography for quantitative measurements of two-dimensional strain distributions *Appl. Opt.* **38** 96–100

[21] Steinchen W, Kupfer G, Mäckel P and Vössing F 1999 Determination of strain distribution by means of digital shearography *Measurement* **26** 79–90

[22] Aebischer H A and Waldner S 1997 Strain distributions made visible with image-shearing speckle pattern interferometry *Opt. Laser. Eng.* **26** 407–20

[23] Groves R M, James S W and Tatam R P 2001 Full surface strain measurement using shearography *Proc. SPIE* **4448** 142–52

[24] Groves R M, James S W and Tatam R P 2000 Polarization-multiplexed and phase-stepped fibre optic shearography using laser wavelength modulation *Meas. Sci. Technol.* **11** 1389–95

[25] Smigielski P, Albe F and Dischli B 1992 Recent advances in interferometric endoscopy *Proc. SPIE* **1755** 61–7

[26] Soloff S M, Adrian R J and Liu Z-C 1997 Distortion compensation for generalized stereoscopic particle image velocimetry *Meas. Sci. Technol.* **8** 1441–54

[27] Shang H M, Hung Y Y, Luo W D and Chen F 2000 Surface profiling using shearography *Opt. Eng.* **39** 23–31

[28] Huang J-R, Ford H D and Tatam R P 1997 Slope measurement by two-wavelength electronic shearography *Opt. Laser. Eng.* **27** 321–33

[29] He Y M, Tay C J and Shang H M 1999 Digital phase-shifting shearography for slope measurement *Opt. Eng.* **38** 1586–90

[30] Groves R M, James S W and Tatam R P 2004 Shape and slope measurement by source displacement in shearography *Opt. Laser. Eng.* **41** 621–34

[31] Anand A, Groves R M, Schwab X, Pedrini G and Osten W 2007 Fresnel wavefront propagation model for shearography shape measurement *Proc. SPIE* **6617** 66170Q

[32] Valera J D R and Jones J D C 1995 Vibration analysis by modulated time-averaged speckle shearing interferometry *Meas. Sci. Technol.* **6** 965–70

[33] Davies J C and Buckberry C H 1985 Application of electronic speckle pattern interferometry in automotive product development *VDI Ber.* **617** 279–93

[34] Huang J-R, Ford H D and Tatam R P 1996 Heterodyning of speckle shearing interferometers by laser diode wavelength modulation *Meas. Sci. Technol.* **7** 1721–7

[35] Moore A J, Jones J D C and Valera J D R 2001 Dynamic measurements *Digital Speckle Pattern Interferometry and Related Techniques* ed P K Rastogi (Chichester: Wiley)

[36] Bard B A, Gordon G A and Wu S 1998 Laser-modulated phase-stepping digital shearography for quantitative full-field imaging of ultrasonic waves *J. Acoust. Soc. Am.* **103** 3327–35

[37] Mäckel P 2004 Die Shearography: Ein quantitatives Messverfahren zur Schwingungsmessung und zerstörungsfreien Prüfung *Laser-Journal.de* **1** (2) 49–54

[38] Hung Y Y, Shang H M and Yang L X 2003 Unified approach for holography and shearography in surface deformation measurement and nondestructive testing *Opt. Eng.* **43** 1197–207

[39] Atcha H and Tatam R P 1994 Heterodyning of fibre-optic speckle pattern interferometers using laser diode wavelength modulation *Meas. Sci. Technol.* **5** 704–9

[40] Hathaway R B, Hovanesian J D and Hung M Y Y 1997 Residual stress evaluation using shearography with large-shear displacements *Opt. Laser. Eng.* **27** 43–60

[41] Tay C J, Toh S L, Shang H M and Lin Q Y 1994 Direct determination of second order derivatives in plate bending using multiple-exposure shearography *Opt. Laser. Technol.* **26** 91–8

[42] Krishna Mohan N 2000 The influence of multiple-exposure recording on curvature pattern using multi-aperture speckle shear interferometry *Opt. Comm.* **186** 259–63

[43] Murukeshan V M, Keong N C, Krishnakumar V, Seng O L and Asundi A 2001 Double shearography for engineering metrology: optical and digital approach *Opt. Laser. Technol.* **33** 325–8

[44] Wang K, Tieu A K and Li E 2002 Influence of displacement and its first- and second-order derivative components on curvature fringe formations in speckle shearography *Appl. Opt.* **41** 4557–61

[45] Bhaduri B, Kothiyal M P and Krishna Mohan N 2007 Curvature measurement using three-aperture digital shearography and fast Fourier transform *Opt. Laser. Eng.* **45** 1001–4

[46] Tay C J and Fu Y 2005 Determination of curvature and twist by digital shearography and wavelet transforms *Opt. Lett.* **30** 2873–5

[47] Fomitchov P A and Krishnaswamy S 1997 A compact dual-purpose camera for shearography and electronic speckle-pattern interferometry *Meas. Sci. Technol.* **8** 581–3

[48] Groves R M, Fu S, James S W and Tatam R P 2005 Single-axis combined shearography and digital speckle photography instrument for full surface strain measurement *Opt. Eng.* **44** 025602

[49] Rosso V, Béland R, Renotte Y, Hebraken S, Lion Y and Charette P 2008 Simultaneous coherent imaging and strain measurement using coupled photorefractive holography and shearography *Opt. Lett.* **33** 797–9

[50] Valera J D R, Jones J D C, Towers D P and Buckberry C H 1997 Strain and vibration analysis by fibre based speckle shearing interferometry *Opt. Laser. Eng.* **26** 361–76

[51] Mihaylova E, Whelan M and Toal V 2004 Simple phase-shifting lateral shearing interferometer *Opt. Lett.* **29** 1264–6

[52] Mihaylova E, Naydenova I, Martin S and Toal V 2004 Electronic speckle pattern shearing interferometer with a photopolymer holographic grating *Appl. Opt.* **43** 2439–42

[53] Zhao S and Chung P S 2006 Digital speckle shearing interferometer using a liquid-crystal spatial light modulator *Opt. Eng.* **45** 105606

[54] Rosso V, Renotte Y, Habraken S, Lion Y, Michel F, Moreau V and Tilkens B 2007 Almost-common path interferometer using the separation of polarization states for digital phase-shifting shearography *Opt. Eng.* **46** 105601

[55] Kurtz R M, Piliavin M A, Pradhan R D, Aye T M, Savant G D, Jannson T P and Hergert S 2004 Reflection shearography for nondestructive evaluation *Proc. SPIE* **5422** 532–40

[56] Falldorf C, Osten W and Kolenovic E 2003 Speckle shearography using a multiband light source *Opt. Laser. Eng.* **40** 543–52

[57] Wang K F and Tieu A K 2004 Theory and experiment of spatially and temporally partially coherent speckle shearing interferometry *Opt. Laser. Technol.* **36** 43–5

[58] Wu T, Jones J D C and Moore A J 2006 High-speed phase-stepped digital speckle pattern interferometry using a complementary metal-oxide semiconductor camera *Appl. Opt.* **45** 5845–55

[59] Groves R M, Pedrini G and Osten W 2008 Real-time extended dynamic range imaging in shearography *Appl. Opt.* **47** 5550–6

[60] Groves R M, Osten W, Doulgeridis M, Kouloumpi E, Green T, Hackney S and Tomari V 2007 Shearography as part of a multi-functional sensor for the detection of signature features in movable cultural heritage *Proc. SPIE* **6618** 661810

[61] Slettemoen G Å 1980 Electronic speckle pattern interferometric system based on a speckle reference beam *Appl. Opt.* **19** 616–23

[62] Huang J-R, Ford H D and Tatam R P 1996 Phase-stepped speckle shearing interferometry by source wavelength modulation *Opt. Lett.* **21** 1421–3

[63] Wyant J C 1974 Use of an ac heterodyne lateral shear interferometer with real-time wavefront correction systems *Appl. Opt.* **14** 2622–6

[64] Hariharan P, Oreb B F and Eiju T 1987 Digital phase shifting interferometry: a simple error compensating algorithm *Appl. Opt.* **26** 2504–6

[65] Carré P 1966 Installation et utilization du comparateur photoélectric et interférentiel du Bureau International des Pois et Mesures *Metrologia* **2** 13–23

[66] Huntley J M 2001 Automated analysis of speckle interferograms *Digital Speckle Pattern Interferometry and Related Techniques* ed P K Rastogi (Chichester: Wiley)

[67] Kujawinska M 1993 Spatial phase measurement methods *Interferogram Analysis, Digital Fringe Pattern Measurement Techniques* ed D W Robinson and G T Reid (Bristol: Institute of Physics Publishing)

[68] García B B, Moore A J, Pérez-López C, Wang L and Tschudi T 1999 Spatial phase-stepped interferometry using a holographic optical element *Opt. Eng.* **38** 2069–74

[69] Millerd J, Brock N, Hayes J, North-Morris M and Wyant J C 2004 Pixelated phase-mask dynamic interferometer *Proc. SPIE* **5531** 304–14

[70] Somers P A A M and Bhattacharya N 2007 Handling unfavourable polarization states in a polarization-based shearing speckle interferometer *J. Opt. A: Pure Appl. Opt.* **9** S92–7

[71] Somers P A A M and Bhattacharya N 2005 Maintaining sub-pixel alignment for a single-camera two-bucket shearing speckle interferometer *J. Opt. A: Pure Appl. Opt.* **7** S385–91

[72] Takeda M, Ina H and Kobayashi S 1982 Fourier-transform method of fringe pattern analysis for computer-based topography and interferometry *J. Opt. Soc. Am.* **72** 156–9

[73] Saldner H O, Molin N-E and Stetson K A 1996 Fourier-transform evaluation of phase data in spatially phase-biased TV holograms *Appl. Opt.* **35** 332–6

[74] Dávila A, Kaufmann G H and Pérez-López C 1998 Transient deformation analysis by a carrier method of pulsed electronic speckle-shearing pattern interferometry *Appl. Opt.* **37** 4116–22

[75] Fernández A, Doval Á F, Kaufmann G H, Dávila A, Blanco-García J, Pérez-López C and Fernández J L 2000 Measurement of transient out-of-plane displacement gradients in plates using double-pulsed subtraction TV shearography *Opt. Eng.* **39** 2106–13

[76] Francis D 2008 Surface strain measurement using pulsed laser shearography with fibre-optic imaging bundles *PhD Thesis* Cranfield University, UK

[77] Pedrini G, Zou Y-L and Tiziani H J 1996 Quantitative evaluation of digital shearing interferogram using the spatial carrier method *Pure Appl. Opt.* **5** 313–21

[78] Santos F, Vaz M and Monteiro J 2004 A new set-up for pulsed digital shearography applied to defect detection in composite structures *Opt. Laser. Eng.* **42** 131–40

[79] Focke O, Hildebrand A and Von Kopylow C 2008 Inspection of laser generated lamb waves using shearographic interferometry *1st Int. Symp. on Laser Ultrasonics: Science, Technology and Applications (Montreal, Canada)*

[80] Francis D, James S W and Tatam R P 2008 Surface strain measurement of rotating objects using pulsed laser shearography with coherent fibre-optic imaging bundles *Meas. Sci. Technol.* **19** 105301

[81] Bhaduri B, Krishna Mohan N, Kothiyal M P and Sirohi R S 2006 Use of spatial phase shifting technique in digital speckle pattern interferometry (DSPI) and digital shearography (DS) *Opt. Exp.* **14** 11598–607

[82] Tay C J, Quan C, Yang F J and He X Y 2004 A new method for phase extraction from a single fringe pattern *Opt. Commun.* **239** 251–8

[83] Kemao Q 2007 Two-dimensional windowed Fourier transform for fringe pattern analysis: principles, applications and implementations *Opt. Laser. Eng.* **45** 304–17

[84] Kemao Q and Soon S H 2007 Sequential demodulation of a single fringe pattern guided by local frequencies *Opt. Lett.* **32** 127–9

[85] Quan C, Fu Y and Miao H 2006 Wavelet analysis of digital shearing speckle patterns with a temporal carrier *Opt. Commun.* **260** 97–104

[86] Aebischer H A and Waldner S 1999 A simple and effective method for filtering speckle-interferometric phase fringe patterns *Opt. Commun.* **162** 205–10

[87] Goldstein R M, Zebker H A and Werner C L 1988 Satellite radar interferometry: two-dimensional phase unwrapping *Radio Sci.* **23** 713–20

[88] Robinson D W 1993 Phase unwrapping methods *Interferogram Analysis, Digital Fringe Pattern Measurement Techniques* ed D W Robinson and G T Reid (Bristol, UK: Institute of Physics)

[89] Sawaf F and Tatam R P 2006 Finding minimum spanning trees more efficiently in tile-based phase unwrapping *Meas. Sci. Technol.* **17** 1428–35

[90] Liu S and Yang L X 2007 Regional phase unwrapping method based on fringe estimation and phase map segmentation *Opt. Eng.* **46** 051012

[91] Huntley J M 2001 Three-dimensional noise immune phase unwrapping algorithm *Appl. Opt.* **40** 3901–8

[92] Dantec Dynamics, Kässbohrerstrasse, Ulm, Germany http://www.dantecdynamics.com/ (accessed on 1 September 2009)

[93] Breuckmann GmbH, Torenstrasse, Meersburg, Germany http://www.breuckmann.com/ (accessed 1 September 2009)

[94] Isi-sys, Wasserweg, Kässel, Germany http://isi-sys.com/html/company_information.html (accessed 25 January 2010)

[95] Waldner S 1996 Removing the image-doubling in shearography by reconstruction of the displacement field *Opt. Commun.* **127** 117–26

[96] Falldorf C, Heimbach Y, von Kopylow C and Jüptner W 2007 Efficient reconstruction of spatially limited phase distributions from their sheared representation *Appl. Opt.* **46** 5038–43

[97] Lee J-R, Yoon D-J, Kim J-S and Vautrin A 2008 Investigation of shear distance in Michelson interferometer-based shearography for mechanical characterization *Meas. Sci. Technol.* **19** 115303

[98] Goto D T and Groves R M 2010 Error analysis of 3D shearography using finite-element modeling *Proc. SPIE* **7718** 771816

[99] James S W, Tatam R P and Elder R L 1997 Design considerations for a three dimensional fiber optic laser Doppler velocimeter for turbomachinery applications *Rev. Sci. Instrum.* **68** 3241–6

[100] Ng T W 1995 Shear measurement in digital speckle shearing interferometry using digital correlation *Opt. Commun.* **115** 241–4

[101] Andersson A, Krishna Mohan N, Sjödahl M and Molin N-E 2000 TV shearography: quantitative measurement of shear magnitude fields by use of digital speckle photography *Appl. Opt.* **39** 2565–8

[102] Wan Abdullah W S and Petzing J N 2005 Development of speckle shearing interferometer error analysis as an aperture function of wavefront divergence *J. Mod. Opt.* **52** 1495–510

[103] Cordero R R and Labbe F 2005 Uncertainty evaluation of displacement gradients measured by electronic speckle pattern shearing interferometry (ESPSI) *Meas. Sci. Technol.* **16** 1315–21

[104] Yang L X, Chen F, Steinchen W and Hung Y Y 2004 Digital shearography for nondestructive testing: potentials, limitations and applications *J. Hologr. Speckle* **1** 69–79

[105] Parker S C J and Salter P L 1999 A novel shearography system for aerospace non-destructive testing *Proc. Inst. Mech. Eng.* **213** 23–33

[106] Huang Y H, Ng S P, Liu L, Li C L, Chen Y S and Hung Y Y 2009 NDT&E using shearography with impulsive thermal stressing and clustering phase extraction *Opt. Laser. Eng.* **47** 774–81

[107] Hung Y Y, Lou W D, Lin L and Shang H M 2000 Evaluating the soundness of bonding using shearography *Compos. Struct.* **50** 353–62

[108] Steinchen W, Yang L, Kupfer G and Mäckel P 1998 Non-destructive testing of aerospace composite materials using digital shearography *Proc. Inst. Mech. Eng.* **212** 21–30

[109] Hung M Y Y, Chen Y S, Ng S P, Shepard S M, Hou Y and Lhota J R 2007 Review and comparison of shearography and pulsed thermography for adhesive bond evaluation *Opt. Eng.* **46** 051007

[110] Hung Y Y, Chen Y S, Ng S P, Liu L, Huang Y H, Luk B L, Ip R W L, Wu C M L and Chung P S 2009 Review and comparison of shearography and active thermography for nondestructive evaluation *Mater. Sci. Eng.* R **64** 73–112

[111] Růžek R, Lohonka R and Jironč J 2006 Ultrasonic C-Scan and shearography NDI techniques evaluation of impact defects detection *NDT&E Int.* **39** 132–42

[112] Kalms M and Osten W 2003 Mobile shearography system for the inspection of aircraft and automotive components *Opt. Eng.* **42** 1188–96
[113] http://isi-systems.com/isi-sys-english/applications/glare/glare-plate.htm (accessed on 1 September 2009)
[114] Pendurangan P and Buckner G D 2007 Defect identification in GRID-LOCK® joints *NDT&E Int.* **40** 347–56
[115] Huang S J and Lin Y T 2008 Out-of-plane strain measurement in sandwich plates with single fully potted insert by using digital shearography *Strain* **44** 253–8
[116] Hung Y Y and Ho H P 2005 Shearography: an optical measurement technique and applications *Mater. Sci. Eng.* **R49** 61–87
[117] Groves R M, Pradarutti B, Kouloumpi E, Osten W and Notni G 2009 2D and 3D non-destructive testing of a wooden panel painting using shearography and terahertz imaging *NDT&E Int.* **42** 543–9
[118] Steinchen W, Kupfer G and Mäckel P 2002 Full field tensile strain shearography of welded specimens *Strain* **38** 17–26
[119] Groves R M, James S W and Tatam R P 2003 Pipe weld investigation using shearography *Strain* **39** 101–5
[120] Groves R M, Furfari D, Barnes S E, James S W, Fu S, Irving P E and Tatam R P 2006 Full-field laser shearography instrumentation for the detection and characterization of fatigue cracks in titanium 10-2-3 *J. ASTM. Int.* **3** JAI-12757
[121] Dilhaire S, Jorez S, Cornet A, Patiño Lopez L D and Claeys W 2000 Measurement of the thermomechanical strain of electronic devices by shearography *Microelectron. Reliab.* **40** 1509–14
[122] Udupa G, Ngoi B K A, Freddy Goh H C and Yusoff M N 2004 Defect detection in unpolished Si wafers by digital shearography *Meas. Sci. Technol.* **15** 35–43
[123] Mihaylova E and Toal V 2009 Simple versatile shearing interferometer for measurements on a microscopic scale *Opt. Laser. Eng.* **47** 271–3
[124] Kumar U P, Kothiyal M P and Krishna Mohan N 2009 Microscopic TV shearography for characterization of microsystems *Opt. Lett.* **34** 1612–4
[125] Sujatha N U and Murukeshan V M 2004 Nondestructive inspection of tissue/tissue like phantom curved surfaces using digital speckle shearography *Opt. Eng.* **43** 3055–60
[126] Murukeshan V M and Sujatha N 2007 All fiber based multispeckle modality endoscopic system for imaging medical cavities *Rev. Sci. Instrum.* **78** 053106
[127] Q-800 Brochure. Dantec Dynamics, Kässbohrerstrasse, Ulm, Germany, Downloaded from http://www.dantecdynamics.com/Default.aspx?ID=672 (accessed 7 September 2009)
[128] Steinbichler Optotechnik, Georg-Wiesboeck Ring, Neubeuern, Germany http://www.steinbichler.de/en/main/isis.htm (accessed 7 September 2009)
[129] Optonor AS, Harald Haarfagres gate 5, Trondheim, Norway http://www.optonor.no/Non-destructive.aspx (accessed 7 September 2009)
[130] Isi-sys, Wasserweg, Kässel, Germany http://www.isi-sys.com/html/piezoshaker.html (accessed 7 September 2009)
[131] Laser Optical Engineering Ltd, Loughborough, Leicestershire, UK http://www.laseroptical.co.uk/ (accessed 7 September 2009)
[132] Laser Technology Inc., West Germantown Pike, Norristown, PA, USA http://www.laserndt.com/ (accessed 7 September 2009)